Dispersion Analysis of Composite Acousto-Elastic Waveguides

Ali Vaziri Astaneh, Murthy N. Guddati*

Department of Civil Engineering, North Carolina State University, Raleigh, NC 27695-7908, USA

Abstract

Propagation characteristics of guided waves are widely utilized for nondestructive characterization of laminated composites which are often immersed in fluid. These propagation characteristics are quantified through dispersion and attenuation curves, and need to be computed for a large number of estimated structure and material property combinations, over a wide range of frequencies. To solve this central problem, an efficient approach is proposed for dispersion analysis of three types of immersed waveguides: laminated plates; laminated rods and pipes; composite waveguides with generic crosssection. The approach is based on Semi-Analytical Finite Element (SAFE) method enhanced with two novel discretization methods: Complex-length Finite Element Method (CFEM) for the solid domain and Perfectly Matched Discrete Layers (PMDL) for the surrounding fluid. The resulting approach is computationally more efficient than the existing methods in that it keeps the underlying eigenvalue problem linear and substantially smaller. The paper presents the basic ideas of the proposed approach, specific algorithms for determining the discretization parameters, and open-source implementation of the resulting waveguide models. Several numerical examples are presented to illustrate the method's efficiency. Finally, the theoretical predictions from the method are validated using experimental observations for several structural members.

Keywords: Layered Structures, Laminates, Computational Modeling, Non-destructive Testing.

1. Introduction

Guided waves are widely used for non-destructive evaluation [1-8] and structural health monitoring [9-12], with specific applications that include corrosion screening of oil and gas pipelines [13-18], characterization of moduli, damage and delamination of composites [19-32], characterization of fluid loaded on structures [33-36], near surface geophysics and earthquake engineering [37-40] as well as ultrasound imaging of biological structures such as arteries [41-43]. The attractiveness of guided waves stems from their long-distance propagation without substantial attenuation. However, in many circumstances, waveguides are immersed in fluid [44-48] or embedded in solid [49-56], resulting in energy loss into the surrounding medium, leading to significant reduction of inspection range. Thus, special attention is given to open

^{*} Corresponding author. Tel.: +1 919 515 7699; fax: +1 919 515 7908 E-mail address: murthy.guddati@ncsu.edu

waveguides in obtaining accurate estimates of attenuation, phase and group velocities, which is termed as dispersion analysis and is the focus of this paper.

In recent years, several methods have been developed for dispersion analysis of acousto-elastic (immersed elastic) waveguides. Examples include analytical methods that have been extensively applied to simple geometries such as plates [57-64] and cylindrical structures [65-71]. Analytical methods are typically based on transfer matrix method [72-74] or global matrix method [75-77]. This family of matrix methods is not computationally demanding; however, its application is limited to simple geometries and solution becomes more complicated by considering multiple layers. Besides, the required root-finding procedure (especially for leaky or damped modes) may fail at high frequencies (see e.g. Figure 6.3 in [78]). Improved root-finding algorithms have been suggested (e.g. in [79]), but require increased computational effort.

Unlike analytical methods, numerical approaches based on finite element semi-discretization are versatile in modeling waveguides with arbitrary geometry, boundary conditions and material property distribution. This family of methods appears to have been first proposed in geotechnical earthquake engineering and geophysics, i.e. the Thin Layer Method (TLM) [80, 81], and extended to ultrasonic applications under the name of Semi-Analytical Finite Element (SAFE) method [82-87]. The idea is to discretize the cross-section of the waveguide (in one or two dimensions) using finite element method (FEM), and use analytical solution along the axis of the waveguide.

Focusing on immersed waveguides, to model the surrounding fluid, SAFE method has been coupled with different approaches. One scheme couples the boundary element method (BEM) with FEM which is referred to as 2.5D FEM-BEM [88]. This method leads to a nonlinear eigenvalue problem that requires a more expensive solution strategy compared to linear eigenvalue problems. Similarly, using exact boundary condition employed in e.g. [89] requires an iterative solution due to nonlinearity. For the special case of immersed plates, the nonlinear eigenvalue problem can be simplified into a cubic eigenvalue problem using a change of variables [90], which too is computationally expensive.

Other hybrid SAFE methods consist of using non-reflecting boundaries [91] or absorbing layers [33]. These methods require minimal modifications to the existing SAFE codes and have the advantage of keeping the eigenvalue problems linear, which can be solved by standard packages. The disadvantage is that a large region of the surrounding fluid has to be discretized, which significantly increases the cost of the eigenvalue problem.

Motivated by eliminating the drawbacks of the existing approaches, we propose an efficient approach for modeling different types of acousto-elastic waveguides, namely (a) immersed laminated plates; (b) immersed laminated rods and fluid-filled pipes; and (c) composite waveguides with generic cross-sections. Specifically, we focus on the discretization of the surrounding infinite fluid and incorporate the method of Perfectly Matched Discrete Layers (PMDL) [92, 93] into the SAFE formulation. PMDL can be considered as an efficient discretization of the highly successful perfectly matched layers (PML, [94]). For each class of waveguides, we examine the underlying wave propagation characteristics and provide simple guidelines for choosing the PMDL parameters. Through several numerical examples, we show that the proposed approach results in accurate dispersion curves with just a handful of PMDL elements, leading to reduced computational cost.

In a second, complementary contribution, we adapt the recently developed Complex-length Finite Element Method (CFEM) [95, 96] for efficient discretization of the interior solid. CFEM is applicable to cross-sections that can be divided into homogeneous intervals (in 1D) or parallelograms (in 2D), and is shown to have convergence properties identical to expensive spectral finite elements, but achieved with

minimal modification to inexpensive linear finite elements. In cases where CFEM is not applicable, we utilize higher order finite elements to discretize the interior (the details are discussed in the appropriate sections).

Finally, the methods resulting from combining the ideas of PMDL, CFEM and high-order FEM are implemented into an open-source software named WaveDisp [97] which computes the dispersion and attenuation curves for various types of waveguides. As illustrated later in the paper, the resulting dispersion curves are verified to be highly accurate, and validated with experimental observations.

2. Overview

In this paper we address dispersion analysis of acousto-elastic waveguides. Specifically, we consider three different cases shown in Figure 1, i.e. immersed plates, immersed rods and fluid-filled pipes and immersed waveguides with generic cross-section. In all cases, solid domain and the infinite fluid medium are semi-discretized using the framework of semi-analytical finite element (SAFE) method.

Discretization of solid domain is performed by the recently developed complex-length finite element method (CFEM), which uses linear midpoint-integrated 1D/2D finite elements with specially designed set of complex-valued lengths. CFEM has shown to provide exponential convergence [95, 96], and can be used for 1D discretization of plates and 2D discretization of waveguides with cross-section that can be divided into parallelograms. For more complicated 2D sections (e.g. with curves boundaries) regular high-order finite elements are used.

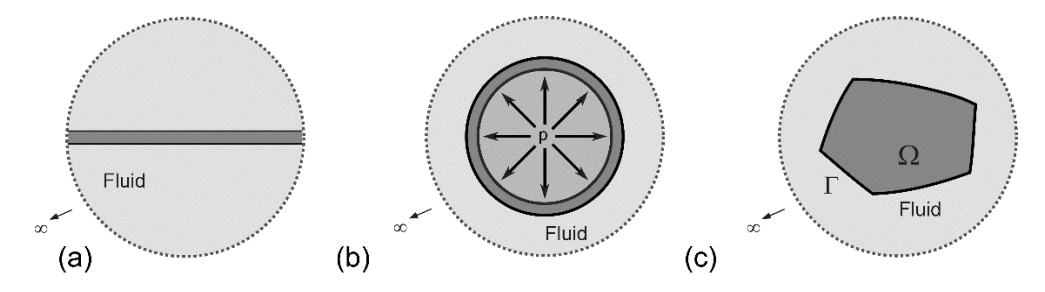


Figure 1 Overview of the studied systems: (a) immersed plates; (b) immersed rods/fluid-filled pipes; and (c) immersed waveguides with arbitrary cross-section.

The infinite fluid is modeled using perfectly matched discrete layers (PMDL), which are mid-point integrated finite elements with real/imaginary lengths that result in exponentially convergent approximation of the exterior impedance [92, 93]. For each problem shown in Figure 1, we separately present the PMDL parameter choice for different combinations of solid and surrounding liquid.

Summary of the proposed algorithms for different waveguides is as follows,

- (a) *Immersed plates*: CFEM is used for 1D discretization of the plate in the thickness direction, along with PMDL layers for modeling the infinite fluid half-spaces outside the plate. Details are given in Section 3.
- (b) *Immersed rods and fluid-filled pipes*: High-order FEM is used for 1D radial discretization of the solid and the fluid inside, along with PMDL for modeling the infinite fluid around the pipe/rod. Details are given in Section 4.

(c) *Immersed waveguides with general section*: The solid domain, and the fluid inside, if any, are discretized in 2D with CFEM (when applicable) or high-order FEM. Fluid PMDL elements are used around the solid domain to represent the unbounded fluid. Details are given in Section 5.

Implementation details for each of the three cases can be found in the open-source software WaveDisp [97], verification studies are presented in respective sections, and validation is presented in Section 6.

3. Plates Immersed in Fluid

As mentioned in the introduction, numerical methods based on SAFE and FEM have been extensively used for investigation of composite structures (see e.g. [5, 98-110]). In this section, we present a brief summary of the SAFE formulation for immersed plates shown in Figure 1 (a). We then classify the solid-born wavemodes into different types and present the appropriate scheme to treat each type of these modes.

3.1 Governing equations

The geometry of the immersed plate is shown in Figure 2 (a). In the solid domain, elastodynamic equation for harmonic response of the form $\tilde{\mathbf{u}}(z,y,t) = \mathbf{u}(z,y,\omega)e^{-i\omega t}$, without external body forces and damping, can be written as,

$$-\mathbf{L}_{\sigma}^{T}\mathbf{\sigma}-\rho_{S}\omega^{2}\mathbf{u}=\mathbf{0},\tag{1}$$

where $\omega \in \mathbb{R}$ is the temporal frequency and $\mathbf{u} = \{u_z \ u_y\}^T$ is the infinitesimal displacement vector. The stress vector $\mathbf{\sigma} = \mathbf{D}\mathbf{\varepsilon} = \{\sigma_{zz} \ \sigma_{yy} \ \sigma_{zy}\}^T$ is related to the strain vector $\mathbf{\varepsilon} = \mathbf{L}_{\varepsilon}\mathbf{u} = \{\varepsilon_{zz} \ \varepsilon_{yy} \ \gamma_{zy}\}^T$ through $\mathbf{D}_{3\times3}$ where the nonzero entries for an isotropic medium are $D_{11} = D_{22} = \rho_S c_p^2$, $D_{33} = \rho_S \ c_s^2$ and $D_{12} = D_{21} = \rho_S \ (c_p^2 - 2c_s^2)$. Parameters c_s and c_p are the shear and pressure wave velocity and ρ_S is the solid density. The nonzero entries of the 3×2 matrix operators \mathbf{L}_{σ} and \mathbf{L}_{ε} are defined as,

$$\mathbf{L}_{\sigma}(\cdot) = \mathbf{L}_{\varepsilon}(\cdot) = \mathbf{L}_{z}^{s} \partial(\cdot) / \partial z + \mathbf{L}_{y}^{s} \partial(\cdot) / \partial y,$$

$$\mathbf{L}_{z}^{s}(1,1) = \mathbf{L}_{z}^{s}(3,2) = 1, \text{ and } \mathbf{L}_{y}^{s}(2,2) = \mathbf{L}_{y}^{s}(3,1) = 1.$$
(2)

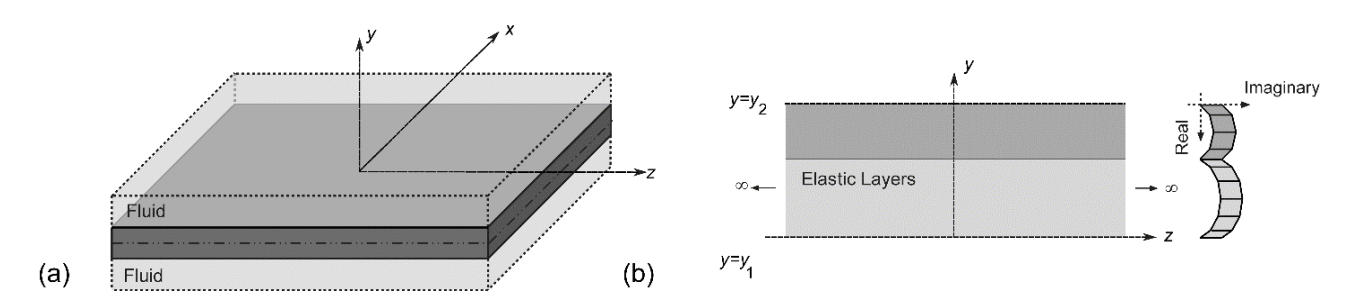


Figure 2 (a) Geometry of the immersed plate; and (b) CFEM discretization of the composite plate.

In fluid domain, equation of motion for the harmonic waves of the form $\tilde{p}(z, y, t) = p(z, y, \omega)e^{-i\omega t}$ can be written as,

$$-\rho_F^{-1} \nabla^2 p - (\omega^2 / \rho_F c_F^2) p = 0, \tag{3}$$

where p is the pressure field and $\nabla^2(\cdot) = \partial^2(\cdot)/\partial z^2 + \partial^2(\cdot)/\partial y^2$. Parameters ρ_F and c_F are the density and pressure wave velocity of the fluid medium respectively.

SAFE framework consists of discretizing the governing equations (1) and (3) in the y direction, but using analytical solution in the z direction (hence the name semi-analytical finite element method -SAFE). As such, the eigenvalue problem associated with the immersed plate can be obtained as,

$$\begin{pmatrix} k_z^2 \begin{bmatrix} \mathbf{K}_2^S & \mathbf{0} \\ \mathbf{0} & \kappa \mathbf{K}_2^F \end{bmatrix} + \begin{bmatrix} \mathbf{K}_0^S - \omega^2 \mathbf{M}^S & -\kappa \mathbf{C}_{SF} \\ -\omega^2 \mathbf{C}_{SF}^T & \kappa (\mathbf{K}_0^F - \omega^2 \mathbf{M}^F) \end{bmatrix} \end{pmatrix} \begin{cases} \mathbf{\phi}_S \\ \mathbf{\phi}_F \end{cases} = \begin{cases} \mathbf{0} \\ \mathbf{0} \end{cases}, \tag{4}$$

where k_z is the wavenumber in the z direction, and $\kappa = \|\mathbf{K}_2^S\|_{\inf} / \|\mathbf{K}_2^F\|_{\inf}$ is the normalization factor that improves the conditioning of the system. Contribution matrices from solid domain \mathbf{K}_2^S , \mathbf{K}_0^S , \mathbf{M}^S , from fluid medium \mathbf{K}_2^F , \mathbf{K}_0^F , \mathbf{M}^F and the fluid-structure interaction matrix \mathbf{C}_{SF} are defined in Appendix A.

To obtain the dispersion and attenuation curves, the wavenumber k_z should be computed by solving the eigenvalue problem (4) for different frequencies. Dispersion curves are often presented as phase velocities for different modes, $c_{\rm ph}^{\rm i} = \omega/\Re(k_z^{\rm i})$, plotted as a function of frequency. Attenuation curves are plotted as the imaginary part of the wavenumbers, i.e. $\alpha^{\rm i} = \Im(k_z^{\rm i})$.

By writing (4) in the form $\mathbf{K}\boldsymbol{\phi}_{\mathrm{R}} = \mathbf{0}$, or $\boldsymbol{\phi}_{\mathrm{L}}^{\dagger}\mathbf{K} = \mathbf{0}$ where $\mathbf{K}(\omega, k_z) = k_z^2 \overline{\mathbf{A}} + \overline{\mathbf{C}}$ and $\boldsymbol{\phi}_{\mathrm{R}}$, $\boldsymbol{\phi}_{\mathrm{L}}$ are the right and left eigenvectors, group velocity can be obtained as,

$$c_{g} = -\Re\left(\frac{\mathbf{\phi}_{L}^{\dagger}(\partial \mathbf{K}/\partial k_{z})\mathbf{\phi}_{R}}{\mathbf{\phi}_{L}^{\dagger}(\partial \mathbf{K}/\partial \omega)\mathbf{\phi}_{R}}\right). \tag{5}$$

Note that $\overline{\mathbf{A}}$ and $\overline{\mathbf{C}}$ can be both functions of frequency, e.g. in the contexts of viscoelasticity and frequency-dependent absorbing layers. It is worth mentioning that eigenvalue derivatives can be also obtained without computing the eigenvectors using the perturbation approach presented in Equation (10) of [40].

3.2 Proposed numerical techniques: CFEM and PMDL

Formulation in (1)-(5) is valid irrespective of the numerical discretization employed in the y direction. We propose to use two different discretization techniques for computational efficiency: (a) the solid plate is discretized using the recently developed Complex-length Finite Element Method (CFEM), and (b) the fluid is discretized using Perfectly Matched Discrete Layers (PMDL), which is effective in modeling wave propagation in unbounded domains. The two methods are summarized in the remainder of the section.

Complex-length Finite Element Method (CFEM): CFEM involves discretizing each homogeneous layer with simple piecewise linear finite elements with two important modifications: (a) midpoint integration is

used to compute element contribution matrices, and (b) the element depths are chosen as specially computed complex values linked to Padé approximants, resulting in mapping of the mesh into the complex plane (see Figure 2(b)). These modifications result in exponential convergence of the dispersion curves with respect to discretization size (as opposed to the algebraic convergence of regular finite element discretization). As a consequence, for a given accuracy, CFEM reduces the size of the eigenvalue problem drastically while preserving the sparsity of the contribution matrices. Further details of the mathematical formulation and the effectiveness of CFEM can be found in [95].

Perfectly Matched Discrete Layers (PMDL): To model the infinite fluid half-spaces, we adopt perfectly matched discrete layers (PMDL) [92], which is a discrete variant of the highly successful perfectly matched layers (PML). PMDL is similar to CFEM in that complex-length linear elements are used with midpoint integration, resulting in exponential convergence; often a handful of PMDL layers are sufficient to discretize the entire unbounded domain. However, unlike CFEM which has a fixed algorithm for choosing complex-valued element lengths, PMDL lengths must be chosen based on the underlying physics. Fortunately, PMDL provides a simple mathematical framework to facilitate the choice of lengths, as described below.

Choice of PMDL parameters: The accuracy of PMDL can be evaluated with the help of the reflection coefficient R, which is the ratio of the amplitude of artificial reflections to that of the incident wave. For n_P PMDL elements, the reflection coefficient for acoustics equation (3) is given by [93],

$$R = \prod_{j=1}^{n_{\rm p}} \left| \frac{k_y - 2i / L_j}{k_y + 2i / L_j} \right|. \tag{6}$$

where $i=\sqrt{-1}$. Clearly, choosing $L_j=2i/k_y^*$ makes the reflection coefficient zero for the specific mode $k_y=k_y^*$. Note that for absorbing the transmitted modes in fluid, one needs to make the reflection coefficient small for multiple modes simultaneously. For propagating waves (with real k_y), the product can be made small by choosing imaginary-valued L_j . Therefore, one can choose the imaginary lengths as $L_j=2i/k_y^j$, which makes the reflection coefficient zero for the reference wavenumbers k_y^j and small enough for the desired range of k_y . In contrast, for evanescent waves (with imaginary k_y) real-valued L_j would be appropriate. It is best to choose these real lengths as $L_j=L_1\alpha^{j-1}$ where α is the geometric ratio (analysis is presented in [111]). Thus, the choice of PMDL parameters are determined by the characteristics of wave propagation into the fluid. Thus, we first examine the wave behavior and then revisit the choice of PMDL parameters.

3.3 Characteristics of solid-born wavemodes

To determine the behavior of wavemodes at the solid-fluid interface, we first drive the dispersion relation in the fluid domain. By taking Fourier transform from (3) in the y and z directions, we obtain,

$$k_{v}^{2} + k_{z}^{2} = (\omega / c_{f})^{2}. \tag{7}$$

where k_y is the vertical wavenumber in the fluid domain. It is well-known that the type of the transmitted waves in the fluid domain depends on the relative properties of the solid and surrounding fluid. If the shear wave velocity in solid is greater than the acoustic velocity in the fluid, solid-born wavemodes are leaky (propagating energy into the fluid). Following [64], we refer to this combination as *hard* solid-fluid interface. In contrast, when the shear wave velocity in solid is less than the acoustic wave velocity in the fluid, solid-born wavemodes are non-leaky or trapped (purely evanescent perpendicular to interface) and we refer to it as *soft* solid-fluid interface. Note that (7) is more complicated than it appears because both k_y and k_z are complex-valued. This is carefully considered in the discussion below and in the references mentioned therein.

At hard solid-fluid interfaces, the transmitted waves into fluid region are leaky in the supersonic zone, i.e. $c_{\rm ph} > c_f$ (see e.g. [64, 90]). From (7), the vertical wavenumber in fluid can be obtained as $k_y = \pm (\omega^2/c_f^2 - k_z^2)^{1/2}$. In order to choose the correct root for leaky Lamb waves, one can consider the top half-space (y > 0) and examine the input power to the fluid domain, i.e.,

$$P = \Re(\mathbf{p}^{\dagger} \cdot \mathbf{t}) = \Re((-i\omega p)^{\dagger} \cdot (-ik_{y}p)) = \omega|p|^{2} \Re(k_{y}). \tag{8}$$

Due to leakage of energy from solid region, the power input into the fluid domain has to be positive, dictating that $\Re(k_y) > 0$. For the hard solid-fluid interface, the leaky modes are in fact predominantly propagative, i.e. $|\Re(k_y)| >> |\Im(k_y)|$ (See Figure 3).

Apart from leaky Lamb waves, two important non-leaky wavemodes exist in the subsonic zone $(c_{\rm ph} < c_f)$: Scholte and quasi-Scholte modes, which are purely evanescent perpendicular to the interface, i.e. $\Re(k_y) = 0$ or $\Im(k_z) = 0$ (see e.g. [90]). Scholte wave propagates along the interface with the constant (Scholte) wave velocity $c_{\rm Sch}$ which is slightly less than c_f . The quasi-Scholte mode, however, is dispersive at lower frequencies but then becomes nondispersive and propagates with constant $c_{\rm Sch}$ at higher frequencies (see Figure 3).

At the soft solid-fluid interface, there exist non-leaky wavemodes in the subsonic zone $c_{\rm ph} < c_f$, which are purely evanescent perpendicular to the interface (see e.g. [64]). Thus the wavemode characteristics are similar to those of Scholte wavemodes, except for being non-dispersive.

3.3.1 Hard solid-fluid interface

We start with leaky waves at hard solid-fluid interfaces. As mentioned before, k_y is complex but dominantly real and has the form $\Re(k_y^i) = \omega/c_y^i$ with the velocity $c_y^i \ge c_f$ (for different modes). Therefore, PMDL elements with imaginary lengths can efficiently absorb outgoing leaky waves. Specifically, we choose,

$$L_{j} = \frac{2i}{\omega} \frac{c_{f}}{\cos((j-1)\pi/2n_{p})}, \quad j = 1,...,n_{p}.$$
 (9)

where $i=\sqrt{-1}$ and $n_{\rm P}$ is the number of PMDL layers. Note that the above PMDL mesh would perfectly absorb waves propagating at angles $\theta_j=(j-1)\pi/2n_{\rm P}$, which have the phase velocities as $c_y^j=c_f/\cos((j-1)\pi/2n_{\rm P})$ (this follows from relations $k_y^j=\omega/c_y^j$ and $L_j=2i/k_y^j$).

Leaky Lamb wave also exists in the subsonic zone $(c_{\rm ph} < c_f)$, see e.g. [90, 112]. However, it cannot be observed in experiments (with measurements at the interface) since it is highly attenuative along the interface. Instead, the quasi-Scholte mode, which is purely propagative along the interface, is observed (see Figure 6 in [113]). Therefore, we ignore presenting parameters for retrieving the leaky waves in the subsonic zone. Note that PMDL can still be designed to capture these modes, but requires negative real lengths; such unconventional choice is necessitated due to the local growth of wavemodes normal to the interface. This case is not explored further in this paper. More details on the local growth of leaky Lamb wave are given in [48, 56, 64, 88, 91, 114-118].

Scholte and quasi-Scholte wavemodes render k_y to be purely imaginary. Scholte waves propagate with constant Scholte wave velocity $c_{\rm Sch}$ (see Figure 3). By substituting $k_z = \omega/c_{\rm Sch}$ in (7), solving for k_y and using $L_j = 2i/k_y^j$, we obtain $L^{\rm Sch} = 2c_f(2\gamma)^{-1/2}/\omega$ where $\gamma = (c_f - c_{\rm Sch})/c_{\rm Sch}$. Note that using one layer with $L^{\rm Sch}$ can accurately retrieve the Scholte wavemode.

The quasi-Scholte mode is dispersive at the beginning, and then the phase velocity converges to $c_{\rm Sch}$ (see Figure 3). Therefore, we need multiple layers with the minimum length (L_1) and gradual increase using $L_j = L_1 \, \alpha^{j-1} \, (j \geq 2)$. To obtain the approximate minimum length, we assume the phase velocity in the dispersive region to have the form $c_{\rm ph} = c_f \, (\omega/\,\omega_0)^{1/2} \,$ where $\omega_0 = c_f^2 \, (c_p^2 h^2 (1-2\upsilon)/12(1-\upsilon)^2)^{-1/2} \,$ is the coincidence frequency (the frequency that $c_{\rm ph} = c_f$) by approximating the plate as a beam. Average mechanical properties of the plate (c_p,υ) can be used for obtaining ω_0 . Note that making these approximations is justified since for the quasi-Scholte mode we use more than one layer, which eventually leads to accurate solution. Using the suggested functional form for $c_{\rm ph}$ and by substituting $k_z = \omega/\,c_{\rm ph}$ in (7), solving for k_y and using $L_j = 2i/\,k_y^j$, the minimum length (which happens at $\omega = \omega_0/2$) takes the form $L_1^{\rm q-Sch} = 4c_f/\omega_0$. In summary, PMDL elements for modeling Scholte and quasi-Scholte waves can be chosen as,

$$L_{j}^{\text{Sch}} = 2c_{f}(2\gamma)^{-1/2} / \omega, \quad \gamma = (c_{f} - c_{\text{Sch}}) / c_{\text{Sch}}, \quad j = 1,$$

$$L_{j}^{\text{q-Sch}} = L_{1}^{\text{q-Sch}} \alpha^{j-1}, \quad L_{1}^{\text{q-Sch}} = 4c_{f} / \omega_{0}, \quad j = 1, ..., n_{p},$$
(10)

where α is the geometric ratio and $c_{\rm Sch}$ can be computed from the closed-from expressions (see e.g. [119]). Note that since retrieving Scholte and quasi-Scholte modes requires real lengths, one can combine the two meshes presented in (10) to obtain both wavemodes accurately and simultaneously.

Filtering criteria: To obtain the leaky waves in the supersonic zone, only complex wavenumbers k_z with $c_f < \omega / \Re(k_z) < c_{\rm ph}^{\rm max}$ should be considered. For non-leaky (Scholte and quasi-Scholte) waves, only purely real wavenumbers k_z with $\omega / k_z < c_f$ need to be considered.

3.3.2 Soft solid-fluid interface

Non-leaky modes at soft solid-fluid interfaces (see e.g. Figure 4) are purely evanescent in the vertical direction and PMDL elements with real length should be used. In this case, it can be shown that the minimum length is required for the first mode at the highest desired frequency. This mode reaches the Scholte wave velocity as frequency increases, therefore by substituting $k_z = \omega_{\rm max} / c_{\rm Sch}$ in (7), solving for k_y and using the PMDL correlation $L = 2i/k_y$, the minimum length can be obtained as $L_1 = 2c_f \left((c_f / c_{\rm Sch})^2 - 1 \right)^{-1/2} / \omega_{\rm max}$. As more than one PMDL element is needed, the length can be increased using,

$$L_i = L_1 \alpha^{j-1} \text{ with } L_1 = 2c_f ((c_f / c_{Sch})^2 - 1)^{-1/2} / \omega_{max}, \quad j = 1, ..., n_P.$$
 (11)

where α is the geometric ratio and ω_{\max} is the maximum frequency of interest for obtaining the dispersion curves.

Similar to hard solid-fluid interfaces, leaky modes exist in the subsonic zone, however only non-leaky waves can be experimentally observed as they propagate with no attenuation along the interface (see Figure 4 in [120]). Thus we ignore the leaky waves in the subsonic zone; if needed, PMDL elements with imaginary lengths should be used for retrieving these modes.

Filtering criteria: To obtain the non-leaky waves in the subsonic zone, only purely real wavenumbers k_z with $\omega/k_z < c_f$ have to be considered.

3.4 Numerical examples

3.4.1 Hard solid plate immersed in fluid

In the first example, we consider a tri-laminate plate immersed in motor oil. Layer materials and thicknesses are given in Table 1. The material properties are reported in Table 2 and used for all the examples in the paper.

Table 1 Parameters of the tri-laminate immersed plate in motor oil. Complex element lengths for a unit-thickness layer is given in Table 1 of [96]. These vales should be simply multiplied by the actual thickness of each layer.

Layer number	Material	h (mm)
-	Motor oil	
1	Titanium	2
2	Brass	2
3	Titanium	1
	Motor oil	∞

Figure 3 compares the dispersion and attenuation curves obtained using (a) the proposed approach of combined CFEM+PMDL discretization, and (b) reference solution obtained using much more expensive approach of combining high-order FEM for the solid plates (11-noded, 10^{th} order finite element for each layer), with the exact impedance condition for the fluid [90]. For the proposed approach, we use 5, 5 and 3 CFEM elements for discretizing the plate layers according to Table 1. For modeling the leaky waves in the fluid half-space, 2 PMDL elements are used on both sides. In a separate analysis, for retrieving the non-leaky modes, we used 1 PMDL element for the Scholte mode along with 2 PMDL elements for the quasi-Scholte mode (using $\alpha = 3$ in (10)). It should be emphasized that even though all the modes are plotted in the same figure, leaky modes are obtained separately using PMDL elements with imaginary lengths and non-leaky (Scholte and quasi-Scholte) modes are obtained using PMDL elements with real lengths.

Table 2 Material properties.

Material	c_s (m/s)	c_p or c_f (m/s)	ρ (kg/m ³)
Stainless Steel SU-304	3200	5900	7840
Aluminum Alloy 6061	3097	6149	2700
Titanium	3230	6060	4460
Brass	2200	4400	8400
Borosilicate Glass D263T	3463	5722	2510
Plexiglass [®]	1200	2500	1180
Lexan®	800	1700	1200
Motor oil	-	1740	870
Water	-	1478	998

Remark on computational cost: If the plate is discretized with n nodes, the exact impedance condition (presented in [90]) leads to a generalized eigenvalue problem of size 4n+2. Whereas using PMDL elements leads to solving a generalized eigenvalue problem of the size 2n+2p where 2p is the total number of PMDL elements for both (top and bottom) half-spaces. It can be seen that by using 2 layers (p=2), PMDL usage leads to solving an eigenvalue problem of roughly half the size. Usage of CFEM further reduces the computational cost, either by reducing n in comparison with finite elements, or increasing sparsity in comparison with spectral elements (see [95, 96] for further discussion).

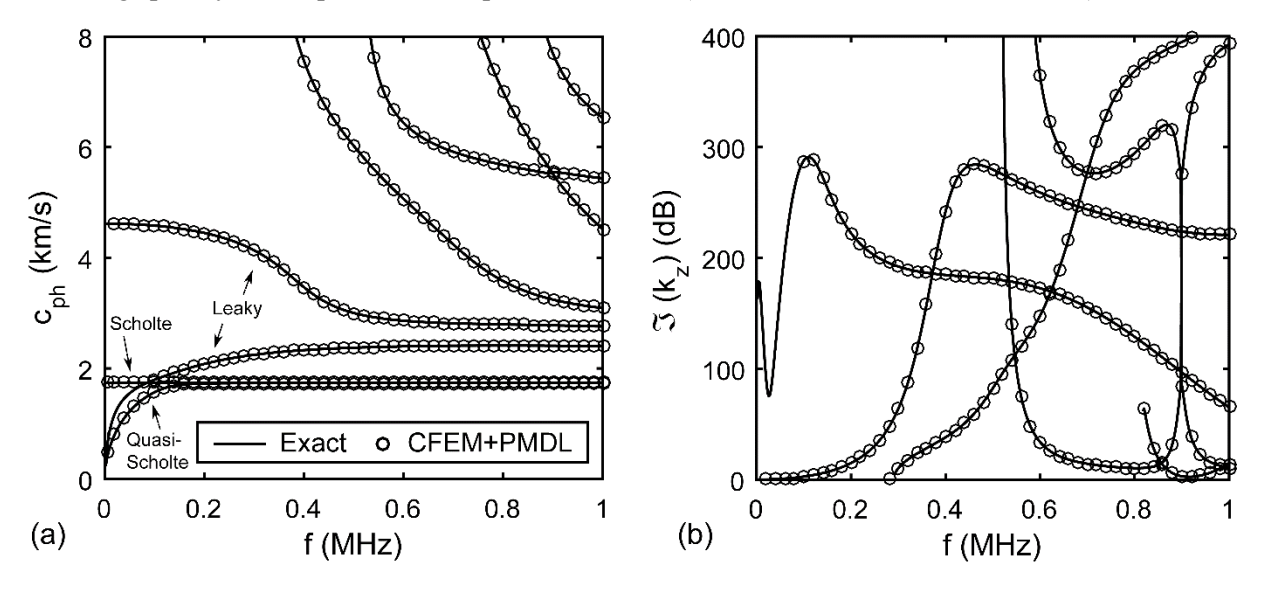


Figure 3 (a) Phase velocity and (b) attenuation curves obtained by the reference solution [90] and the proposed approach (CFEM+PMDL) for the tri-laminate hard plate (Table 1).

3.4.2 Soft solid plate immersed in fluid

We now consider a tri-laminate made up of flexible materials as shown in Table 3 (material properties are given in Table 2).

Table 3 Parameters of a tri-laminate immersed plate in motor oil.

Layer number	Material	h (mm)
-	Motor oil	∞
1	Lexan®	2
2	Plexiglass [®]	2
3	Lexan®	1
-	Motor oil	∞

As shown in Figure 4, CFEM+PMDL discretization leads to accurate phase and group velocity curves when compared to the reference solution [90], again obtained by discretizing each layer with an 11-noded 10^{th} order finite element. For the proposed approach, 5, 5 and 3 CFEM elements are used for the plate, and 4 real-length PMDL elements are used for the fluid (with $\alpha = 4$ in (11)). The group velocities are calculated using Equation (5). Note that there is no need to plot attenuation curves for soft-solid cases because there is no leakage of energy into the fluid and thus no attenuation along the waveguide.

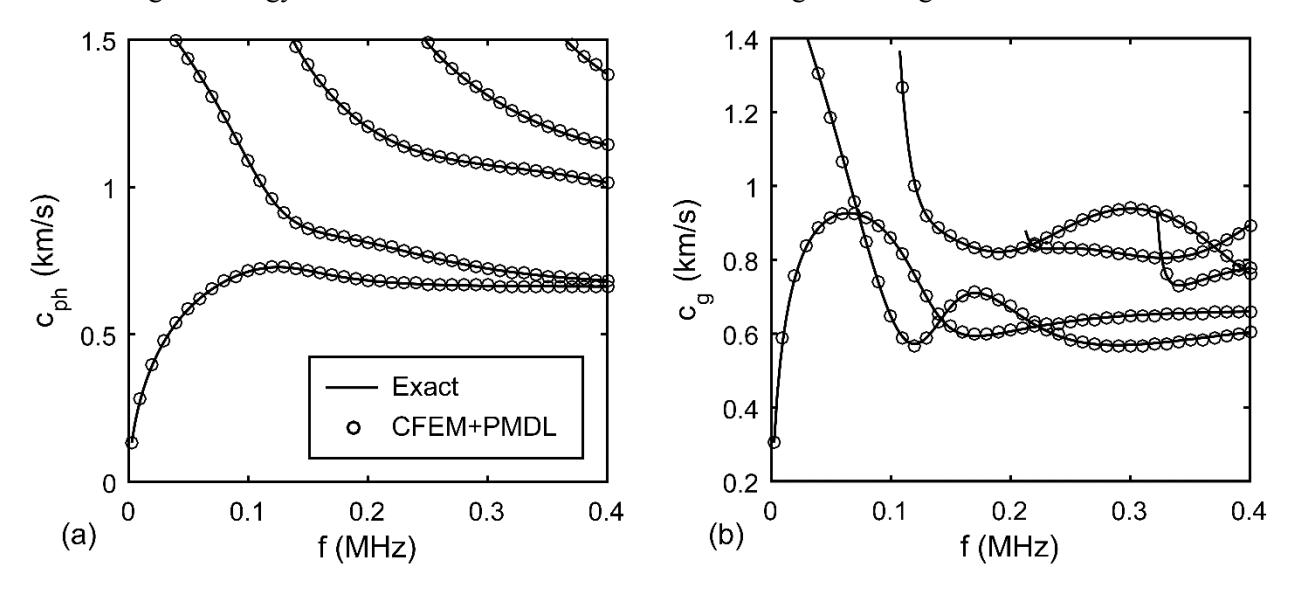


Figure 4 (a) Phase velocity and (b) group velocity curves obtained by the reference solution [90] and the proposed approach (CFEM+PMDL) for the tri-laminate soft plate (Table 3).

4. Immersed rods and (fluid-filled) pipes

4.1 Governing equations

The geometry of the immersed cylindrical waveguide is shown in Figure 5 (a). In the solid domain, elastodynamic equation for the harmonic waves of the form $\tilde{\mathbf{u}}(\mathbf{x},t) = \mathbf{u}(\mathbf{x},\omega)e^{-i\omega t}$ with $\mathbf{x} = (r,\theta,z)$ is given in (1). In this problem, $\mathbf{u} = \{u_r \ u_\theta \ u_z\}^T$ is the displacement vector and the stress vector $\mathbf{\sigma} = \mathbf{D}\mathbf{\varepsilon} = \{\sigma_{rr} \ \sigma_{\theta\theta} \ \sigma_{zz} \ \sigma_{\theta z} \ \sigma_{rz} \ \sigma_{r\theta}\}^T$ is related to the strain vector $\mathbf{\varepsilon} = \mathbf{L}_{\varepsilon}\mathbf{u} = \{\varepsilon_{rr} \ \varepsilon_{\theta\theta} \ \varepsilon_{zz} \ \gamma_{\theta z} \ \gamma_{rz} \ \gamma_{r\theta}\}^T$ through $\mathbf{D}_{6\times6}$ where the nonzero entries for an isotropic medium are $D_{11} = D_{22} = D_{33} = \rho_S \ c_p^2$, $D_{44} = D_{55} = D_{66} = \rho_S \ c_s^2$ and $D_{12} = D_{21} = D_{13} = D_{31} = D_{23} = D_{32} = \rho_S \ (c_p^2 - 2c_s^2)$. The nonzero entries of 6×3 matrix operators \mathbf{L}_{σ} and \mathbf{L}_{ε} are,

$$\mathbf{L}_{\sigma}(\cdot) = \mathbf{L}_{r}^{S} r^{-1} \partial(\cdot \times r) / \partial r + \mathbf{L}_{\theta}^{S} r^{-1} \partial(\cdot) / \partial \theta + \mathbf{L}_{z}^{S} \partial(\cdot) / \partial z - \mathbf{L}_{\sigma}^{S} r^{-1},$$

$$\mathbf{L}_{\varepsilon}(\cdot) = \mathbf{L}_{r}^{S} \partial(\cdot) / \partial r + \mathbf{L}_{\theta}^{S} r^{-1} \partial(\cdot) / \partial \theta + \mathbf{L}_{z}^{S} \partial(\cdot) / \partial z + \mathbf{L}_{\sigma}^{S} r^{-1},$$

$$\mathbf{L}_{r}^{S}(1,1) = \mathbf{L}_{r}^{S}(5,3) = \mathbf{L}_{r}^{S}(6,2) = 1, \text{ and } \mathbf{L}_{\theta}^{S}(2,2) = \mathbf{L}_{\theta}^{S}(4,3) = \mathbf{L}_{\theta}^{S}(6,1) = 1,$$

$$\mathbf{L}_{z}^{S}(3,3) = \mathbf{L}_{z}^{S}(4,2) = \mathbf{L}_{z}^{S}(5,1) = 1, \text{ and } \mathbf{L}_{\sigma}^{S}(2,1) = -\mathbf{L}_{\sigma}^{S}(6,2) = 1.$$

$$(12)$$

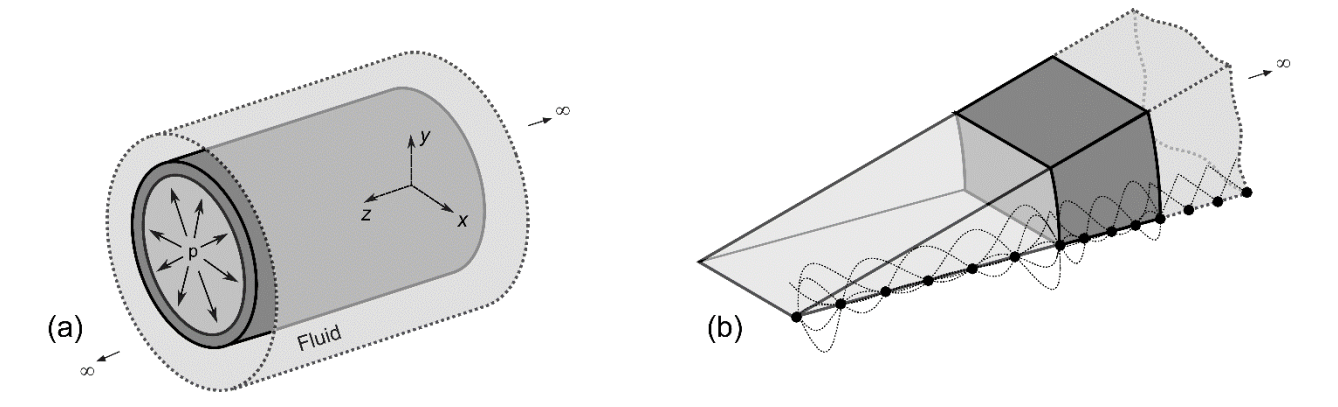


Figure 5 (a) Geometry of the immersed pipe; and (b) 1D discretization of solid and inner fluid with high-order finite elements and linear PMDL elements for the exterior infinite fluid.

In the fluid domain, equation of motion for the harmonic waves of the form $\tilde{p}(\mathbf{x},t) = p(\mathbf{x},\omega)e^{-i\omega t}$ is given in (3) with $\nabla^2(\cdot) = r^{-1}\partial(r \times \partial(\cdot)/\partial r)/\partial r + r^{-2}\partial^2(\cdot)/\partial \theta^2 + \partial^2(\cdot)/\partial z^2$.

SAFE approach for cylindrical waveguides consists (a) using Fourier series expansion in the azimuthal direction, (b) discretizing the solid and fluid governing equations (1) and (3) in the radial direction, and (c) analytical solution in the longitudinal direction. The resulting eigenvalue problem is similar to (4) where the contribution matrices for the cylindrical waveguide, namely \mathbf{K}_2^S , \mathbf{K}_0^S , \mathbf{M}^S , \mathbf{K}_2^F , \mathbf{K}_0^F , \mathbf{M}^F and \mathbf{C}_{SF} are defined in Appendix B.

Purely circumferential wavemodes: The formulation presented in this section corresponds to longitudinal wavemodes. However, as discussed in [78], simple modifications can be considered to analyze wavemodes that propagate only along the circumference. To this end, one should eliminate the variation of displacement components in the z direction, implying plane strain condition. Hence, by removing the u_z degrees of

freedom and setting $k_z=0$, eigenvalue problem (4) has to be solved for the circumferential Fourier number n. The circumferential phase velocity at any radius r can be calculated using $c_{\rm ph}=r\times\omega/n$.

4.2 Radial discretization and choice of parameters

As shown in Figure 5 (b), the inner fluid and the cylinder are discretized with high-order finite elements, since CFEM is not applicable in cylindrical coordinates. Also while midpoint integration scheme of PMDL elements is not as beneficial in cylindrical coordinates as it is in Cartesian coordinates, we still advocate using PMDL elements to discretize the infinite fluid along the radius as they are expected to increase the overall accuracy. The choice of PMDL parameters are discussed in the rest of this section.

PMDL parameters for hard solid-fluid interface: Similar to plates, cylindrical leaky waves at the hard solid-fluid interface are dominantly propagative in the radial direction. Therefore, PMDL elements with imaginary length are needed, which can be chosen as,

$$L_{j} = \frac{2i}{\omega(n_{\rm p} + 1 - j)} \frac{c_{f}}{\cos((j - 1)\pi/2n_{\rm p})}, \quad j = 1, ..., n_{\rm p}.$$
(13)

which is similar to (9), except for a factor of $(n_P + 1 - j)$. Based on numerical investigations, such scaling increases the accuracy in cylindrical coordinates. Importantly, due to this, the element lengths become increasingly smaller and finely graded as the number of layers n_P is increased, indicating that PMDL converges to continuous cylindrical PML, which is known to be exact (see e.g. [121]); this indicates that PMDL with parameter choice in (13) converges to the exact solution.

PMDL parameters for soft solid-fluid interface: Similar to plates, the non-leaky waves are purely evanescent in the radial direction and PMDL layers with real lengths should be used as follows:

$$L_{j} = L_{1}\alpha^{j-1} / (n_{p} + 1 - j) \text{ with } L_{1} = 2c_{f}((c_{f} / c_{Sch})^{2} - 1)^{-1/2} / \omega_{max}, \text{ for } j = 1, ..., n_{p}.$$
 (14)

Like with the hard solid-fluid interface, the factor (n+1-j) helps with accuracy and the cylindrical PMDL converges to the exact solution.

Note that the filtering criteria for plates, as mentioned in Section 3.3, hold for cylindrical waveguides as well.

4.3 Numerical examples

4.3.1 Hard solid pipe in fluid

A tri-laminate pipe is considered, with layer properties shown in Table 4. The pipe is filled with and immersed in motor oil. As mentioned before, material properties are given in Table 2.

Table 4 Parameters of a tri-laminate hard pipe filled with and immersed in motor oil.

Layer number	Material	$r_{\rm in}$ (mm)	$r_{\rm out}$ (mm)
200) 01 11011110 01	1.1000011001	in 🔻	out

-	Motor oil	0	5
1	Titanium	5	7
2	Brass	7	9
3	Titanium	9	10
_	Motor oil	10	90

As CFEM is not applicable to this problem, we use regular high-order finite elements to discretize the solid and the inner fluid region. Thus the goal here is to investigate the performance of just the PMDL discretization. Each layer is discretized with an 11-noded element, and five 11-noded elements are used to discretize the fluid inside. We consider 6 PMDL layers based on Equation (13) to model the leaky waves. Figure 6 shows the resulting dispersion and attenuation curves (for the circumferential Fourier number n=1). Also shown in the figure is the reference solution, obtained by the same high-order discretization for the solid and inner fluid region, but with 30 PMDL layers to ensure convergence. Clearly, the proposed discretization results in excellent match with the converged solution.

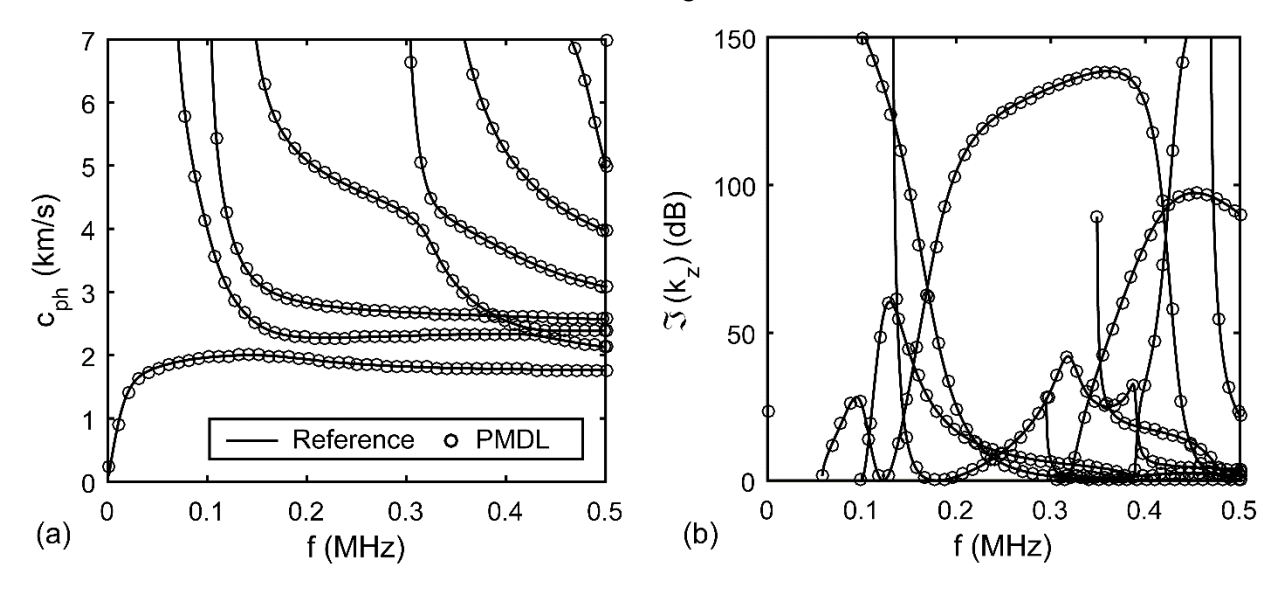


Figure 6 (a) Phase velocity and (b) attenuation curves obtained by the reference solution and proposed approach (PMDL) for the tri-laminate fluid-filled and immersed hard pipe (Table 4).

4.3.2 Soft solid pipe in fluid

We now consider another tri-laminate pipe, but with more flexible materials as shown in Table 5 (material properties are reported in Table 2). The pipe is filled with and immersed in motor oil.

Table 5 Parameters of a tri-laminate soft pipe filled with and immersed in motor oil.

Layer number	Material	$r_{\rm in}$ (mm)	r _{out} (mm)
-	Motor oil	0	5
1	Lexan®	5	7
2	Plexiglass [®]	7	9
3	Lexan®	9	10
-	Motor oil	10	∞

Figure 7 shows the calculated phase and group velocity curves for n=1 (similar to plates, there is no attenuation for soft-solid waveguides). Each of the pipe layers is discretized with one 11-noded finite element, and the inner fluid region is discretized using five 11-noded elements. To model the non-leaky waves we use 5 PMDL elements (with $\alpha = 3$ using (14)). The reference solution is obtained with 30 PMDL elements to ensure convergence. Again, the match between the proposed discretization and the converged solution is excellent.

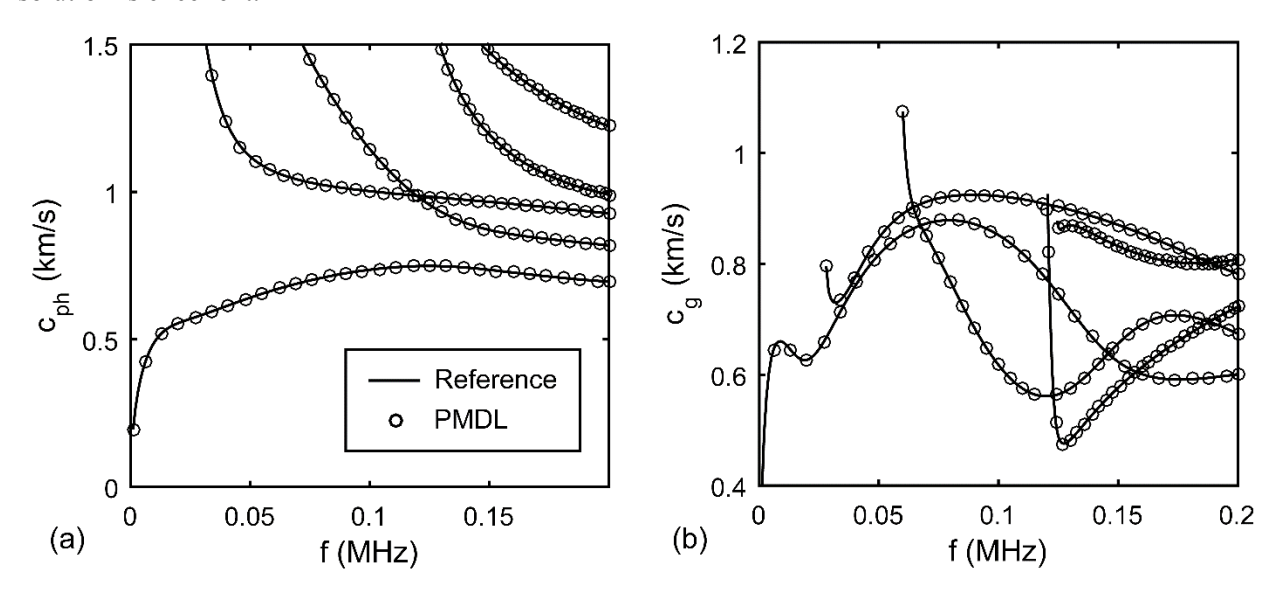


Figure 7 (a) Phase velocity and (b) group velocity curves using the reference solution and proposed approach (PMDL) for the tri-laminate fluid-filled and immersed soft pipe (Table 5).

5. Immersed waveguides with general cross-section

5.1 Governing equations

Geometry of the immersed waveguides with general cross-section is shown in Figure 8 (a). In the solid domain, elastodynamic equation for the harmonic waves of the form $\tilde{\mathbf{u}}(\mathbf{x},t) = \mathbf{u}(\mathbf{x},\omega)e^{-i\omega t}$ with $\mathbf{x} = (x,y,z)$ is given in (1) where, in this problem, $\mathbf{u} = \{u_x \ u_y \ u_z\}^T$ is the displacement vector and the stress vector $\mathbf{\sigma} = \mathbf{D}\mathbf{\varepsilon} = \{\sigma_{xx} \ \sigma_{yy} \ \sigma_{zz} \ \sigma_{yz} \ \sigma_{xz} \ \sigma_{xy}\}^T$ is related to the strain vector $\mathbf{\varepsilon} = \mathbf{L}_{\varepsilon}\mathbf{u} = \{\varepsilon_{xx} \ \varepsilon_{yy} \ \varepsilon_{zz} \ \gamma_{yz} \ \gamma_{xz} \ \gamma_{xy}\}^T$ through $\mathbf{D}_{6\times6}$ where the nonzero entries for an isotropic medium are $D_{11} = D_{22} = D_{33} = \rho_S \ c_p^2$, $D_{44} = D_{55} = D_{66} = \rho_S \ c_s^2$ and $D_{12} = D_{21} = D_{13} = D_{31} = D_{23} = D_{32} = \rho_S \ (c_p^2 - 2c_s^2)$. The nonzero entries of 6×3 matrix operators \mathbf{L}_{σ} and \mathbf{L}_{ε} are,

$$\mathbf{L}_{\sigma}(\cdot) = \mathbf{L}_{\varepsilon}(\cdot) = \mathbf{L}_{x}^{s} \partial / \partial x + \mathbf{L}_{y}^{s} \partial / \partial y + \mathbf{L}_{z}^{s} \partial / \partial z, \text{ with } \mathbf{L}_{x}^{s}(1,1) = \mathbf{L}_{x}^{s}(5,3) = \mathbf{L}_{x}^{s}(6,2) = 1,$$

$$\mathbf{L}_{y}^{s}(2,2) = \mathbf{L}_{y}^{s}(4,3) = \mathbf{L}_{y}^{s}(6,1) = 1, \text{ and } \mathbf{L}_{z}^{s}(3,3) = \mathbf{L}_{z}^{s}(4,2) = \mathbf{L}_{z}^{s}(5,1) = 1.$$

$$(15)$$

In the fluid domain, equation of motion for the harmonic waves of the form $\tilde{p}(\mathbf{x},t) = p(\mathbf{x},\omega)e^{-i\omega t}$ is given in (3) with $\nabla^2(\cdot) = \partial^2(\cdot)/\partial x^2 + \partial^2(\cdot)/\partial y^2 + \partial^2(\cdot)/\partial z^2$.

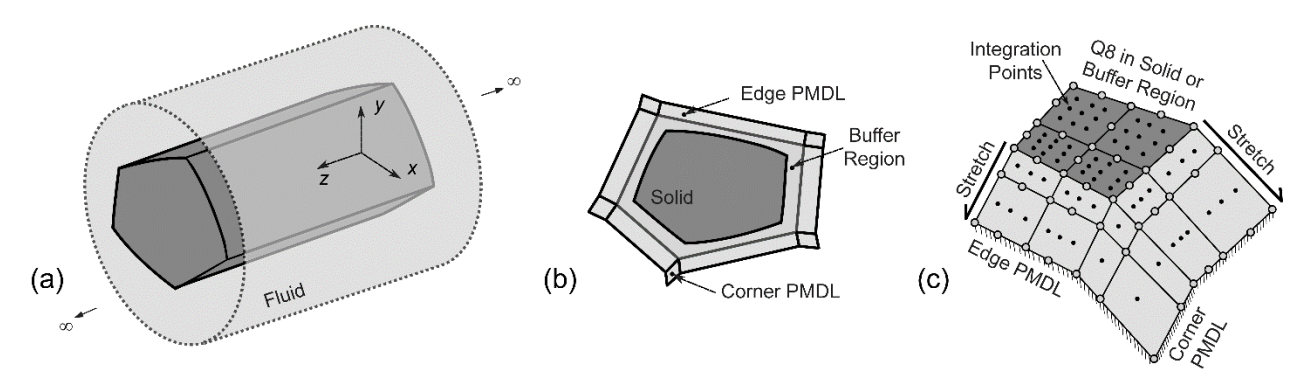


Figure 8 (a) Geometry of the immersed waveguide with arbitrary cross-section; (b) modeling infinite fluid with PMDL layers; and (c) integration scheme for edge and corner PMDL layers.

SAFE approach for three-dimensional waveguides with arbitrary cross-section consists of discretizing the governing equations for solid (1) and fluid (3) in the two-dimensional plane of the cross-section, and using the analytical representation in the longitudinal direction. The resulting eigenvalue problem is similar to (4) where the contribution matrices, namely \mathbf{K}_{2}^{S} , \mathbf{K}_{0}^{S} , \mathbf{M}^{S} , \mathbf{K}_{2}^{F} , \mathbf{K}_{0}^{F} , \mathbf{M}^{F} and \mathbf{C}_{SF} are presented in Appendix C.

5.2 Two-dimensional discretization using CFEM, high-order FEM and PMDL

For two-dimensional discretization, CFEM is applicable to cross-sections that can be split into homogeneous parallelograms. Each parallelogram should be meshed with 4-nonded bilinear finite elements with two modifications: using midpoint (1×1) integration, and choosing the element lengths along each side of the parallelogram from 1D CFEM mesh (see Figure 2 (b)).

Similar to 1D problems, PMDL elements can be used to model the 2D infinite fluid medium, as they are highly efficient for polygonal interiors [93]. Thus, if the solid domain has an arbitrary shape, it has to be surrounded by a buffer (fluid) region, resulting in polygonal computational boundary. Outside the buffer region, PMDL edge and corner elements can be utilized as shown in Figure 8 (b). Note that the buffer region can be minimized by defining a polygon close to the solid domain. This also means that, for polygonal solid domains, a buffer region is not necessary and the PMDL can be placed right next to the solid-fluid interface.

Figure 8 (c) illustrates the details of the edge and corner PMDL elements along with their respective integration schemes. The discretization of the solid domain (and the buffer fluid region) can be performed with any (high-order) finite elements. PMDL edge elements would have the same discretization and integration scheme along the interface. On the other hand, they have linear shape functions and use one integration point in the direction perpendicular to the polygon boundary. Consequently, the corner PMDL elements are 4-noded parallelogram elements with bilinear shape functions and midpoint (1×1) integration

scheme. More details on implementation of PMDL method for two-dimensional problems can be found in [93].

Choice of PMDL parameters: For two-dimensional problems, the PMDL element lengths along the boundary are consistent with interior. Perpendicular to the boundary, the same criterion for 1D plates with hard or soft interface as given in (9) and (11) can be used. Note that the filtering criteria for plates, as mentioned in Section 3.3, hold for waveguides with more general cross-section as well.

5.3 Numerical examples

5.3.1 Hard solid rod in fluid with 2D discretization

We first consider the bi-laminate rod shown in Figure 9 (a) with layer properties given in Table 6 (material properties are reported in Table 2). The waveguide is assumed to be immersed in motor oil. While the radial discretization described in the previous section can be used here, we utilize general two-dimensional discretization proposed in this section to illustrate its performance.

Table 6 Parameters of a bi-laminate immersed hard rod in motor oil

Layer number	Material	$r_{\rm in}$ (mm)	r _{out} (mm)
1	Brass	0	1
2	Titanium	1	2
-	Motor oil	2	∞

The Solid domain and buffer fluid region are discretized with Q8 elements. Thus, PMDL edge and corner elements are 6- and 4-noded elements with quadratic and linear shape functions along and perpendicular to the boundary, respectively (see Figure 8 (c) for description). Note that the buffer region can be minimized by considering a hexagon, but for simplicity we chose a square as shown in Figure 9 (b). Also not considered here is the symmetry that can be used per the approach shown in Figure 4 of [122].

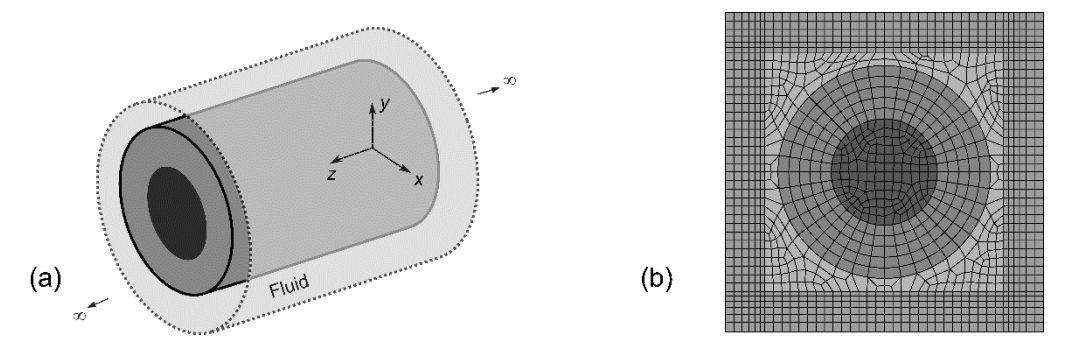


Figure 9 (a) Geometry of the bi-laminate immersed rod; (b) 2D discretization of solid cross-section (with Q8), fluid buffer region (with Q8) and infinite fluid (with PMDL 6-noded edge and 4-noded corner elements). Note that PMDL element lengths perpendicular to the square sides are imaginary and the illustration is schematic.

Figure 10 shows the dispersion and attenuation curves for the leaky wavemodes. The two-dimensional mesh for the cross-section is shown in Figure 9 (b). We used 6 PMDL elements in each stretch direction. The reference solution is obtained by using the 1D cylindrical waveguide model discussed in Section 4 (with 11-noded elements for each layer and 30 PMDL layers for the fluid). Note that the two-dimensional model retrieves all the wavemodes with different circumferential orders. However, in Figure 10, for the sake of clarity, only the modes with circumferential orders n = 0 - 4 are shown. The figure clearly shows good match with the reference solution, indicating the effectiveness of the proposed 2D discretization.

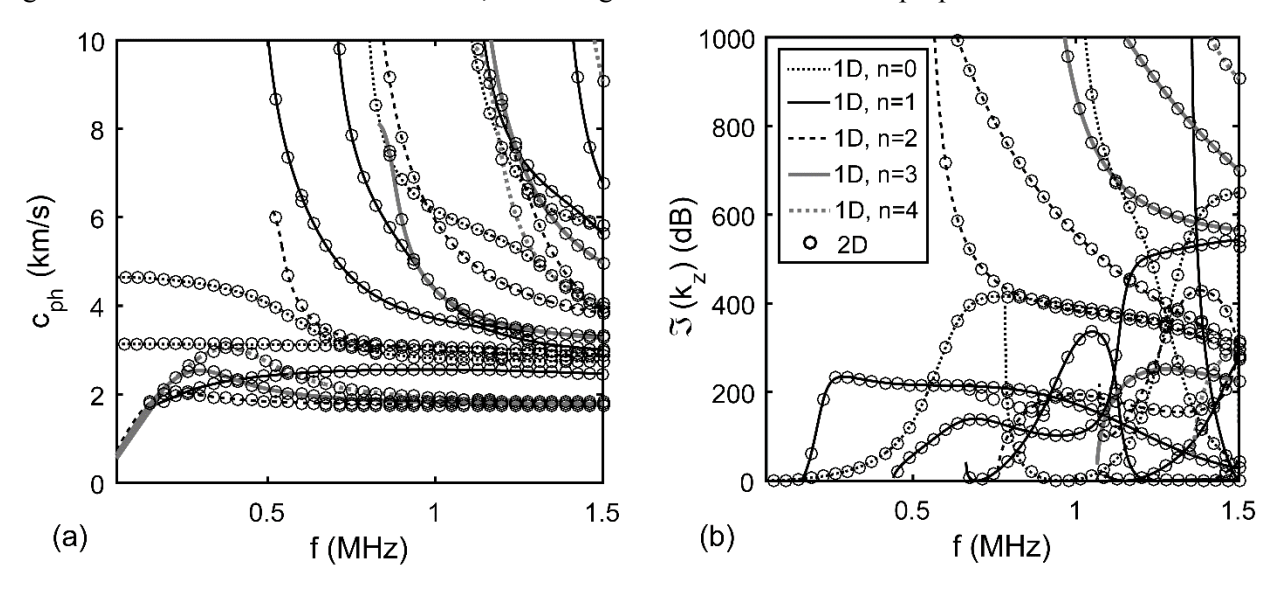


Figure 10 (a) Phase velocity and (b) attenuation curves obtained by the reference solution and proposed approach (PMDL) for the bi-laminate immersed hard rod (Table 6).

5.3.2 Soft solid rod in fluid (rectangular cross-section)

To illustrate the benefits of CFEM in 2D settings, we consider bi-laminate rectangular rod as shown in Figure 11 (a). Layer materials and dimensions are given in Table 7 (again, material properties are reported in Table 2). The waveguide is assumed to be immersed in motor oil.

Table 7 Parameters of a bi-laminate immersed soft rod in motor oil.

104 111 1110101 0111			
Layer number	Material	h (mm)	l (mm)
1	Lexan®	1	2
2	Plexiglass [®]	1	2
-	Motor oil	∞	∞

Since the solid domain in this example can be divided to rectangles, each with constant martial property, we use CFEM for discretization (note that CFEM is applicable whenever we have piecewise homogeneous parallelograms). Also since the solid domain has polygonal shape, no buffer region is included; the PMDL elements are directly connected to the solid-fluid interface. It is also important to note that when CFEM and PMDL elements are used together, the interface integrals (in matrix \mathbf{C}_{SF} of (4)) has to be evaluated with midpoint integration as well.

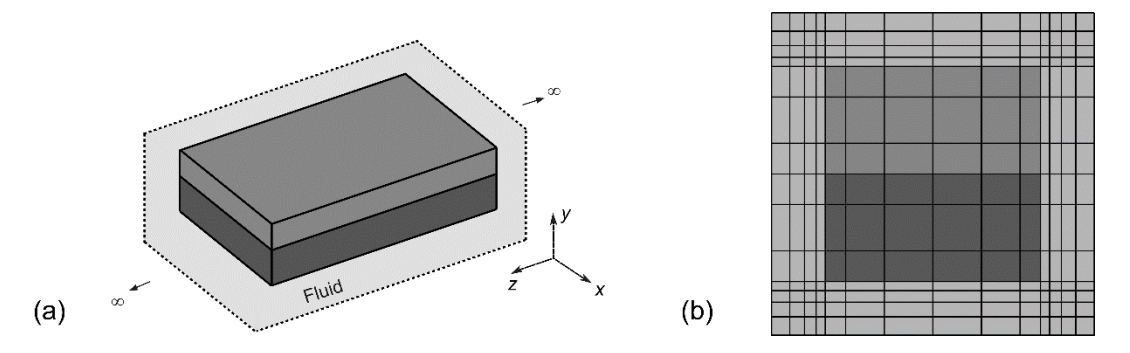


Figure 11 (a) Geometry of the immersed composite rod; (b) 2D discretization of cross-section with 4-noded complex-length elements (only real part is shown) and infinite fluid with 4-noded edge and corner PMDL elements. Note that PMDL element lengths perpendicular to the rod sides are not to scale and the illustration is schematic.

We used 6 CFEM elements in the horizontal direction, and discretized each vertical layer with 3 CFEM elements. Real part of the mesh is shown in Figure 11 (b). The complex-valued mesh in each direction is similar to Figure 2 (b). To model the non-leaky wavemodes, we used 4 PMDL layers (with $\alpha = 3.5$ using (14)). Note that as there are two different solid materials at the solid-fluid interfaces, one can choose $L_1 = \min(L_1^{\text{Plexiglass}}, L_1^{\text{Lexan}})$ to obtain the minimum required length. Reference solution is obtained using a 20×20 Q8 mesh along with 20 PMDL layers to ensure the convergence. Figure 12 shows the resulting phase and group velocity curves, which clearly indicates that the CFEM+PMDL discretization is effective in capturing the dispersion curves.

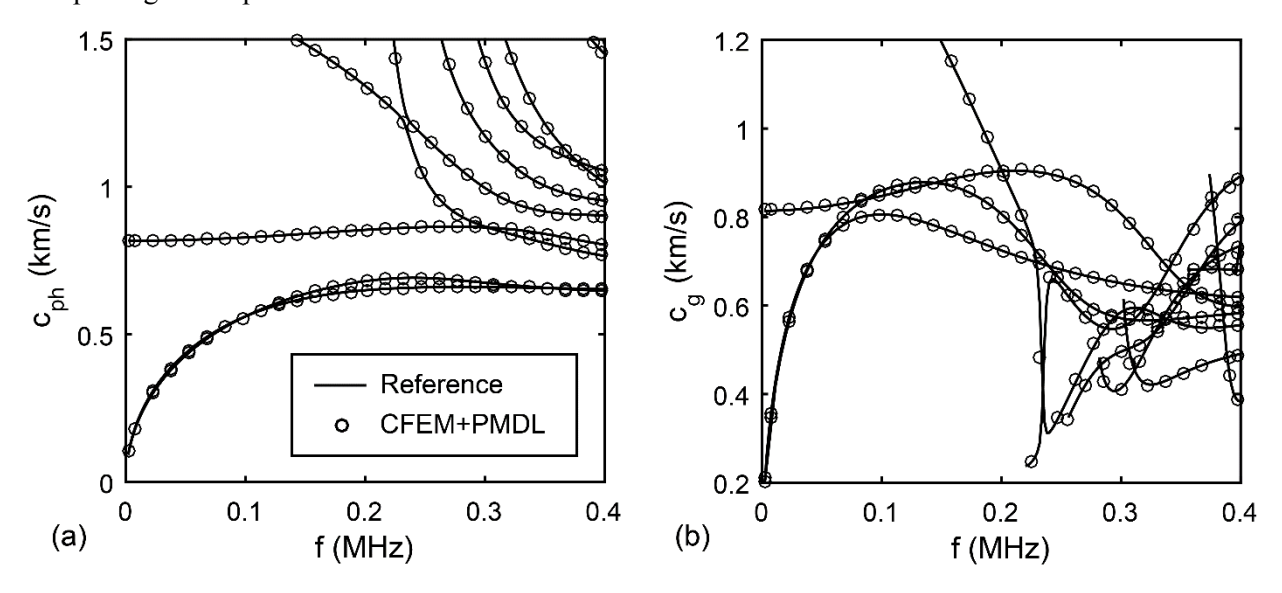


Figure 12 (a) Phase velocity and (b) attenuation curves obtained by the reference solution and proposed approach (PMDL) for the bi-laminate immersed soft rod (Table 7).

6. Validation

In order to validate the proposed computational methods, we compare predictions from the methods with experimental results from the literature. The examples include immersed hard/soft plates, a fluid-filled and immersed pipe and an immersed rectangular rod. As described below, all examples confirm the validity of the proposed waveguide models.

6.1 Immersed plate: hard/soft solid-fluid interface

In the first example we consider two experiments on plates with hard and soft solid-fluid interface which are taken from [123] and [120] respectively. The first experiment was carried out on a 210 µm thick borosilicate glass plate and the second was carried out on a 50 µm thick Plexiglass[®] plate. Both plates were immersed in water, and manufacturer-provided material properties are reported in Table 2.

The glass plate is discretized using 8 CFEM elements and, based on Equation (9), 3 PMDLs are used to model the leaky waves. For the Plexiglass® plate, we used 6 CFEM elements along with 4 PMDLs with $\alpha = 4$ (based on Equation (11)). Figure 13 shows the experimental and theoretical dispersion curves for the two samples. It can be observed that the theoretical predictions match the experimental curves very well.

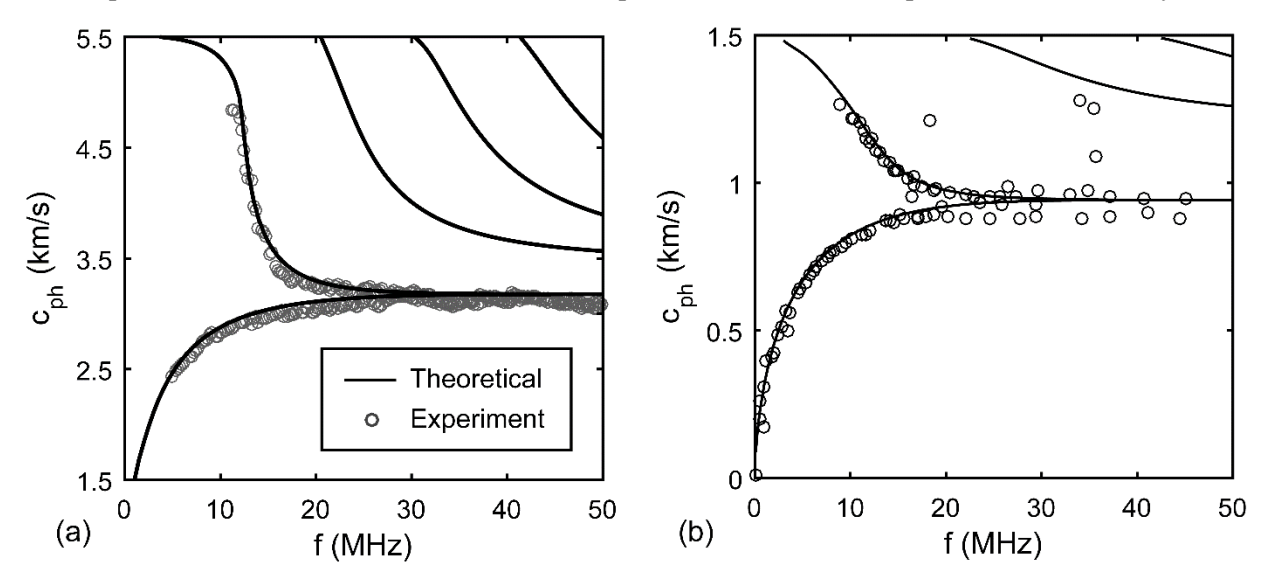


Figure 13 Phase velocity curves for immersed plates, (a) 210 μm thick borosilicate glass plate and (b) 50 μm thick Plexiglass[®] plate, compared with the experimental results from [123] and [120], respectively.

6.2 Immersed fluid-filled pipe: hard solid-fluid interface

To validate the proposed approach for cylindrical waveguides, we use the data from the experiments in [124], carried out on two stainless-steel pipes of 300 µm and 150 µm thickness filled with and immersed in water. Manufacturer-provided material properties are reported in Table 2. In these experiments,

measurements were performed along the perimeter, thus we calculated the phase velocity curves corresponding to circumferential waves at the outer most radius (see Section 4.1 for details).

The solid and inner fluid domain are each discretized with an 11-noded finite element, while 5 PMDLs are used to model the infinite surrounding fluid (based on Equation (13)). As discussed in Section 3.3, to obtain the desired solution i.e. leaky waves, only complex wavenumbers have to be considered. Figure 14 illustrates the experimental and theoretical dispersion curves for the two samples; again, an excellent overall agreement is observed.

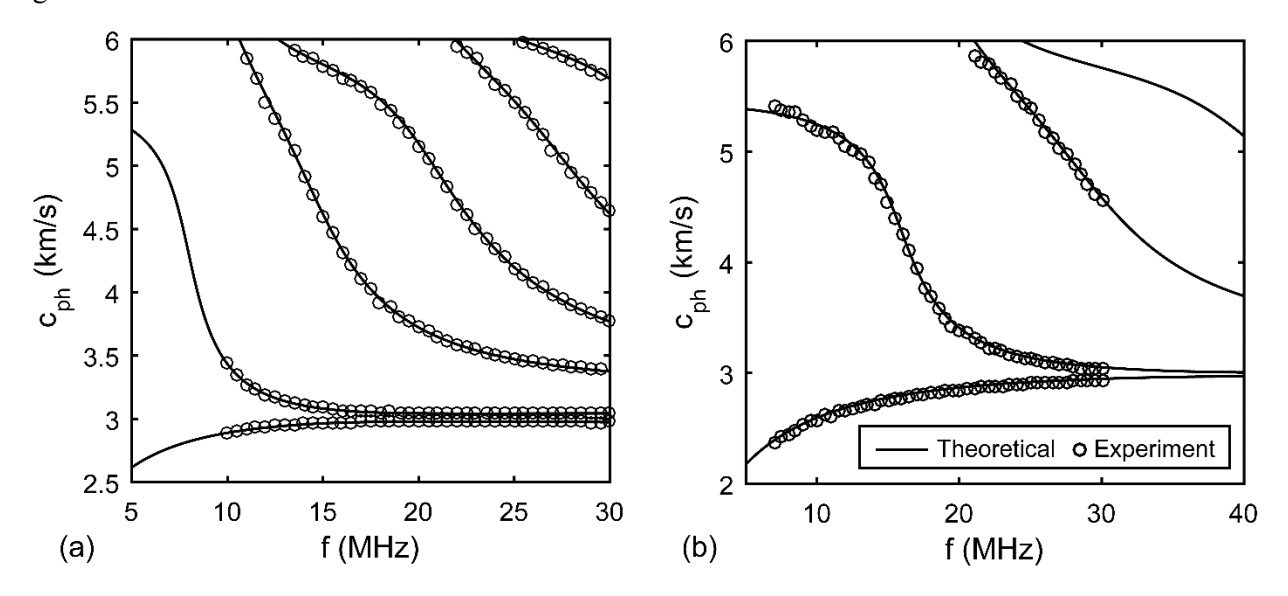


Figure 14 Phase velocity curves for (a) 300 μm and (b) 150 μm immersed stainless steel pipes compared with experimental results from [124].

6.3 Immersed rod: hard solid-fluid interface

In the last validation example, we consider the experiment in [125], carried out on a 3.175×12.700 mm rectangular aluminum rod immersed in water. The manufacturer-provided material properties are given in Table 2. We used a 6×16 CFEM mesh for the rod. The surrounding fluid is discretized with 8 imaginary-length PMDLs, based on Equation (9), and 2 real PMDLs ($L_1 = 1$, $L_2 = 2$ mm) to treat the evanescent waves. In a separate analysis to retrieve the quasi-Scholte wavemode, we used the same discretization for rod along with 4 real PMDL layers based on Equation (10), with $L_1 = 0.1$ mm and $\alpha = 3$. Experimental and theoretical dispersion and attenuation curves are shown in Figure 15, indicating good match between the two for both leaky and quasi-Scholte modes.

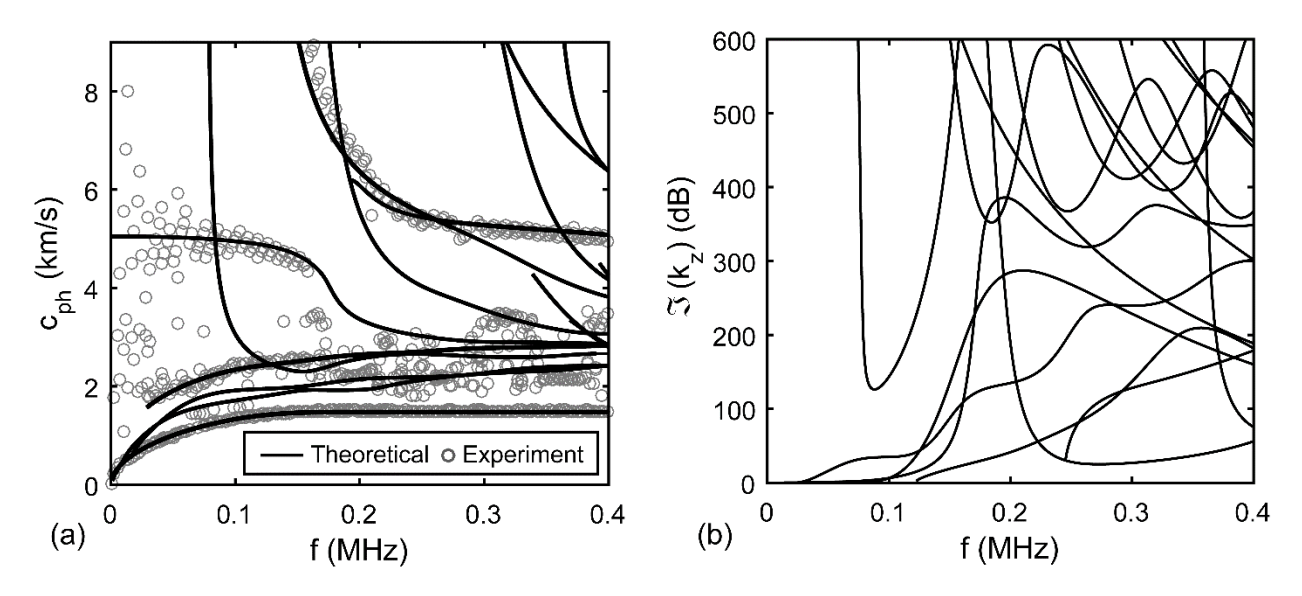


Figure 15 (a) phase velocity and (b) attenuation curves for 3.175×12.700 mm immersed aluminum rod with experimental results from [125].

7. Conclusions

We have proposed an efficient approach for dispersion analysis of different types of composite waveguides immersed in acoustic fluid: plates; circular rods; pipes and fluid-filled pipes; and prismatic waveguides with arbitrary cross-section. The underlying formulation is based on the semi-analytical finite element (SAFE) method, enhanced by recently developed discretization methods to increase the computational efficiency. For discretization of solid domain, we used complex-length finite element method (CFEM). This method provides exponential convergence and is applicable to laminated plate-like structures and the waveguides with cross-section made up of homogeneous parallelograms. Regular high-order finite elements are used for other waveguides with other shapes. Fluid region is discretized using the perfectly matched discrete layers (PMDL), which is an efficient discretization of the PML absorbing boundary condition. We provided approaches for choosing PMDL parameters, as well as simple filtering criteria required for identification of appropriate dispersion curves. The method is implemented in an open-source software named WaveDisp [97].

Using various numerical examples, it is shown that a handful of PMDL elements (and CFEM elements when applicable) are sufficient to obtain accurate dispersion curves, as opposed to large number of traditional finite elements and absorbing layers, thus resulting in significant reduction in the computational cost. The approach is validated for each type of waveguides by comparing with experimentally observed dispersion curves. In each of the three cases, very good agreement was observed. Future work will investigate the application of the methodology to waveguides embedded in infinite solid media.

Acknowledgements

This material is based upon work supported by the National Science Foundation under Grant No. DMS-1016514 and Grant No. CMMI-1635291.

References

- [1] Kundu T. Ultrasonic nondestructive evaluation: engineering and biological material characterization. Boca Raton, FL: CRC press; 2003.
- [2] Liu G-R, Han X. Computational inverse techniques in nondestructive evaluation. Boca Raton, FL: CRC press; 2003.
- [3] Su ZQ, Ye L, Lu Y. Guided Lamb waves for identification of damage in composite structures: A review. J Sound Vibr. 2006;295(3-5):753-80.
- [4] Rose JL. Ultrasonic guided waves in solid media. New York, NY: Cambridge University Press; 2014.
- [5] Jang I, Park I, Lee U. Guided waves in a Timoshenko beam with a bonded composite patch: Frequency domain spectral element modeling and analysis. Compos Pt B-Eng. 2014;60:248-60.
- [6] Liu GR, Lam KY, Shang HM. Scattering of waves by flaws in anisotropic laminated plates. Compos Pt B-Eng. 1996;27(5):431-7.
- [7] Liu Y-C, Huang JH. Dispersion relations and modes of wave propagation in inclusion-reinforced composite plates. Compos Pt B-Eng. 2012;43(3):1649-57.
- [8] Kim BH, Jang JB, Lee HP, Lee DH. Evaluating longitudinal vibration characteristics of bonded strands embedded in prestressed concrete beams by a system identification approach. Compos Pt B-Eng. 2012;43(3):1531-7.
- [9] Rose JL. The upcoming revolution in ultrasonic guided waves. In: Wu H, editor. Nondestructive Characterization for Composite Materials, Aerospace Engineering, Civil Infrastructure, and Homeland Security. San Diego, CA: International Society for Optics and Photonics; 2011. p. 1-30.
- [10] Willberg C, Duczek S, Vivar-Perez JM, Ahmad ZAB. Simulation Methods for Guided Wave-Based Structural Health Monitoring. Appl Mech Rev. 2015;67(1).
- [11] Mitra M, Gopalakrishnan S. Guided wave based structural health monitoring: A review. Smart Mater Struct. 2016;25(5).
- [12] Senthil K, Arockiarajan A, Palaninathan R, Santhosh B, Usha KM. Defects in composite structures: Its effects and prediction methods A comprehensive review. Compos Struct. 2013;106:139-49.
- [13] Na WB, Kundu T. Underwater pipeline inspection using guided waves. J Press Vessel Technol-Trans ASME. 2002;124(2):196-200.
- [14] Ditri JJ. Utilization of guided elastic-waves for the characterization of circumferential cracks in hollow cylinders. J Acoust Soc Am. 1994;96(6):3769-75.
- [15] Lowe MJS, Alleyne DN, Cawley P. Defect detection in pipes using guided waves. Ultrasonics. 1998;36(1-5):147-54.
- [16] Dehghan-Niri E, Salamone S. A multi-helical ultrasonic imaging approach for the structural health monitoring of cylindrical structures. Struct Health Monit. 2015;14(1):73-85.
- [17] Kwun H, Kim SY, Light GM. The magnetostrictive sensor technology for long range guided wave testing and monitoring of structures. Mater Eval. 2003;61(1):80-4.
- [18] Shi JX, Natsuki T, Lei XW, Ni QQ. Wave propagation in the filament-wound composite pipes conveying fluid: Theoretical analysis for structural health monitoring applications. Compos Sci Technol. 2014;98:9-14.
- [19] Hosseini SMH, Willberg C, Kharaghani A, Gabbert U. Characterization of the guided wave propagation in simplified foam, honeycomb and hollow sphere structures. Compos Pt B-Eng. 2014;56:553-66.
- [20] Zhao JL, Qiu JH, Ji HL. Reconstruction of the nine stiffness coefficients of composites using a laser generation based imaging method. Compos Sci Technol. 2016;126:27-34.
- [21] Eremin AA, Glushkov EV, Glushkova NV, Lammering R. Evaluation of effective elastic properties of layered composite fiber-reinforced plastic plates by piezoelectrically induced guided waves and laser Doppler vibrometry. Compos Struct. 2015;125:449-58.
- [22] Yu J, Lefebvre JE, Guo YQ. Free-ultrasonic waves in multilayered piezoelectric plates: An improvement of the Legendre polynomial approach for multilayered structures with very dissimilar materials. Compos Pt B-Eng. 2013;51:260-9.

- [23] Fantuzzi N, Tornabene F. Strong Formulation Isogeometric Analysis (SFIGA) for laminated composite arbitrarily shaped plates. Compos Pt B-Eng. 2016;96:173-203.
- [24] Kundu T, Maslov K, Karpur P, Matikas TE, Nicolaou PD. A Lamb wave scanning approach for the mapping of defects in 0/90 titanium matrix composites. Ultrasonics. 1996;34(1):43-9.
- [25] Scarponi C, Briotti G. Ultrasonic technique for the evaluation of delaminations on CFRP, GFRP, KFRP composite materials. Compos Pt B-Eng. 2000;31(3):237-43.
- [26] Ishak SI, Liu GR, Shang HM, Lim SP. Locating and sizing of delamination in composite laminates using computational and experimental methods. Compos Pt B-Eng. 2001;32(4):287-98.
- [27] Martinez-Jequier J, Gallego A, Suarez E, Javier Juanes F, Valea A. Real-time damage mechanisms assessment in CFRP samples via acoustic emission Lamb wave modal analysis. Compos Pt B-Eng. 2015;68:317-26.
- [28] Hu N, Shimomukai T, Yan C, Fukunaga H. Identification of delamination position in cross-ply laminated composite beams using S-0 Lamb mode. Compos Sci Technol. 2008;68(6):1548-54.
- [29] Esmaeel RA, Taheri F. Delamination detection in laminated composite beams using the empirical mode decomposition energy damage index. Compos Struct. 2012;94(5):1515-23.
- [30] Barbero EJ, Lonetti P, Sikkil KK. Finite element continuum damage modeling of plain weave reinforced composites. Compos Pt B-Eng. 2006;37(2-3):137-47.
- [31] Della CN, Shu D. Vibration of delaminated multilayer beams. Compos Pt B-Eng. 2006;37(2-3):227-36.
- [32] Andrews MG, Massabo R. Delamination in flat sheet geometries with material imperfections and thickness variations. Compos Pt B-Eng. 2008;39(1):139-50.
- [33] Fan Z, Lowe MJS, Castaings M, Bacon C. Torsional waves propagation along a waveguide of arbitrary cross section immersed in a perfect fluid. J Acoust Soc Am. 2008;124(4):2002-10.
- [34] Shepard CL, Burghard BJ, Friesel LA, Hildebrand BP, Xang M, Diaz AA, et al. Measurements of density and viscosity of one- and two-phase fluids with torsional waveguides. IEEE Trans Ultrason Ferroelectr Freq Control. 1999;46(3):536-48.
- [35] Mathieu J, Schweitzer P. Measurement of liquid density by ultrasound backscattering analysis. Meas Sci Technol. 2004;15(5):869-76.
- [36] Ma J, Lowe MJS, Simonetti F. Measurement of the properties of fluids inside pipes using guided longitudinal waves. IEEE Trans Ultrason Ferroelectr Freq Control. 2007;54(3):647-58.
- [37] Nazarian S, Stokoe Ii KH, Hudson WR. Use of spectral analysis of surface waves method for determination of moduli and thicknesses of pavement systems. Transp Res Record. 1983;390:38-45.
- [38] Park CB, Miller RD, Xia J. Multichannel analysis of surface waves. Geophysics. 1999;64(3):800-8.
- [39] Foti S, Lai CG, Rix GJ, Strobbia C. Surface wave methods for near-surface site characterization. Boca Raton, FL: CRC Press; 2014.
- [40] Vaziri Astaneh A, Guddati MN. Improved Inversion Algorithms for Near Surface Characterization. Geophys J Int. 2016;206(2):1410-23.
- [41] Oliver JJ, Webb DJ. Noninvasive assessment of arterial stiffness and risk of atherosclerotic events. Arterioscler Thromb Vasc Biol. 2003;23(4):554-66.
- [42] Hermeling E, Reesink KD, Kornmann LM, Reneman RS, Hoeks APG. The dicrotic notch as alternative time-reference point to measure local pulse wave velocity in the carotid artery by means of ultrasonography. J Hypertens. 2009;27(10):2028-35.
- [43] Dutta P, Urban MW, Le Maitre OP, Greenleaf JF, Aquino W. Simultaneous identification of elastic properties, thickness, and diameter of arteries excited with ultrasound radiation force. Phys Med Biol. 2015;60(13):5279-96.
- [44] Aristegui C, Lowe MJS, Cawley P. Guided waves in fluid-filled pipes surrounded by different fluids. Ultrasonics. 2001;39(5):367-75.
- [45] Fuller CR, Fahy FJ. Characteristics of wave-propagation and energy-distributions in cylindrical elastic shells filled with fluid. J Sound Vibr. 1982;81(4):501-18.
- [46] Han JH, Kim YJ, Karkoub M. Wave propagation modeling of fluid-filled pipes using hybrid analytical/two-dimensional finite element method. Wave Motion. 2014;51(7):1193-208.

- [47] Kochupillai J, Ganesan N, Padmanabhan C. A semi-analytical coupled finite element formulation for shells conveying fluids. Comput Struct. 2002;80(3-4):271-86.
- [48] Hu J, Menyuk CR. Understanding leaky modes: slab waveguide revisited. Adv Opt Photonics. 2009;1(1):58-106.
- [49] Mazzotti M, Bartoli I, Marzani A, Viola E. A coupled SAFE-2.5D BEM approach for the dispersion analysis of damped leaky guided waves in embedded waveguides of arbitrary cross-section. Ultrasonics. 2013;53(7):1227-41.
- [50] Castaings M, Lowe M. Finite element model for waves guided along solid systems of arbitrary section coupled to infinite solid media. J Acoust Soc Am. 2008;123(2):696-708.
- [51] Deng QT, Yang ZC. Wave propagation analysis in buried pipe conveying fluid. Appl Math Model. 2013;37(9):6225-33.
- [52] Gravenkamp H, Birk C, Song CM. Computation of dispersion curves for embedded waveguides using a dashpot boundary condition. J Acoust Soc Am. 2014;135(3):1127-38.
- [53] Jia H, Jing M, Joseph LR. Guided wave propagation in single and double layer hollow cylinders embedded in infinite media. J Acoust Soc Am. 2011;129(2):691-700.
- [54] Leinov E, Lowe MJS, Cawley P. Ultrasonic isolation of buried pipes. J Sound Vibr. 2016;363:225-39.
- [55] Muggleton JM, Yan J. Wavenumber prediction and measurement of axisymmetric waves in buried fluid-filled pipes: Inclusion of shear coupling at a lubricated pipe/soil interface. J Sound Vibr. 2013;332(5):1216-30.
- [56] Nguyen KL, Treyssede F, Hazard C. Numerical modeling of three-dimensional open elastic waveguides combining semi-analytical finite element and perfectly matched layer methods. J Sound Vibr. 2015;344:158-78.
- [57] Bernard A, Lowe MJS, Deschamps M. Guided waves energy velocity in absorbing and non-absorbing plates. J Acoust Soc Am. 2001;110(1):186-96.
- [58] Cegla FB, Cawley P, Lowe MJS. Material property measurement using the quasi-Scholte mode A waveguide sensor. J Acoust Soc Am. 2005;117(3):1098-107.
- [59] Chimenti DE, Rokhlin SI. Relationship between leaky lamb modes and reflection coefficient zeros for a fluid-coupled elastic layer. J Acoust Soc Am. 1990;88(3):1603-11.
- [60] Dayal V, Kinra VK. Leaky lamb waves in an anisotropic plate. I: An exact solution and experiments. J Acoust Soc Am. 1989;85(6):2268-76.
- [61] Nayfeh AH, Chimenti DE. Propagation of guided-waves in fluid-coupled plates of fiber-reinforced composite. J Acoust Soc Am. 1988;83(5):1736-47.
- [62] Shuvalov AL, Poncelet O, Deschamps M. Analysis of the dispersion spectrum of fluid-loaded anisotropic plates: flexural-type branches and real-valued loops. J Sound Vibr. 2006;290(3-5):1175-201.
- [63] Freedman A. Anomalies of the A(0) leaky lamb mode of a fluid-loaded, elastic plate. J Sound Vibr. 1995;183(4):719-37.
- [64] Glorieux C, Van de Rostyne K, Nelson K, Gao WM, Lauriks W, Thoen J. On the character of acoustic waves at the interface between hard and soft solids and liquids. J Acoust Soc Am. 2001;110(3):1299-306.
- [65] Ahmad F. Guided waves in a transversely isotropic cylinder immersed in a fluid. J Acoust Soc Am. 2001;109(3):886-90.
- [66] Baik K, Jiang JA, Leighton TG. Acoustic attenuation, phase and group velocities in liquid-filled pipes: Theory, experiment, and examples of water and mercury. J Acoust Soc Am. 2010;128(5):2610-24.
- [67] Berliner MJ, Solecki R. Wave propagation in fluid-loaded, transversely isotropic cylinders. Part I. Analytical formulation. J Acoust Soc Am. 1996;99(4):1841-7.
- [68] Borgiotti GV, Rosen EM. Power-flow analysis of surface-waves on a cylindrical elastic shell in an acoustic fluid. J Acoust Soc Am. 1994;95(1):244-55.
- [69] Dayal V. Longitudinal-waves in homogeneous anisotropic cylindrical-bars immersed in fluid. J Acoust Soc Am. 1993;93(3):1249-55.
- [70] Nagy PB. Longitudinal guided-wave propagation in a transversely isotropic rod immersed in fluid. J Acoust Soc Am. 1995;98(1):454-7.

- [71] Sato H, Ogiso H. Analytical Method for Guided Waves Propagating in a Fluid-Filled Pipe with Attenuation. Jpn J Appl Phys. 2013;52(7).
- [72] Thomson WT. Transmission of elastic waves through a stratified solid medium. J Appl Phys. 1950;21(2):89-93.
- [73] Haskell NA. The dispersion of surface waves on multilayered media Bull Seismol Soc Amer. 1953;43.1:17-34.
- [74] Nayfeh AH, Nagy PB. General study of axisymmetric waves in layered anisotropic fibers and their composites. J Acoust Soc Am. 1996;99(2):931-41.
- [75] Knopoff L. A matrix method for elastic wave problems. Bull Seismol Soc Amer. 1964;54(1):431-8.
- [76] Lowe MJS. Matrix techniques for modeling ultrasonic-waves in multilayered media. IEEE Trans Ultrason Ferroelectr Freq Control. 1995;42(4):525-42.
- [77] Randall MJ. Fast programs for layered half-space problems. Bull Seismol Soc Amer. 1967;57(6):1299-315.
- [78] Van Velsor JK. Circumferential guided waves in elastic and viscoelastic multilayered annuli. PA, USA: The Pennsylvania State University; 2009.
- [79] Bause F, Walther A, Rautenberg J, Henning B. Reliable Computation of Roots in Analytical Waveguide Modeling Using an Interval-Newton Approach and Algorithmic Differentiation. IEEE Trans Ultrason Ferroelectr Freq Control. 2013;60(12):2597-606.
- [80] Kausel E, Peek R. Dynamic loads in the interior of a layered stratum An explicit solution. Bull Seismol Soc Amer. 1982;72(5):1459-81.
- [81] Tassoulas JL, Kausel E. Elements for the numerical-analysis of wave motion in layered strata. Int J Numer Methods Eng. 1983;19(7):1005-32.
- [82] Datta SK, Shah AH, Bratton RL, Chakraborty T. Wave-propagation in laminated composite plates. J Acoust Soc Am. 1988;83(6):2020-6.
- [83] Gavric L. Computation of propagative waves in free rail using a finite-element technique. J Sound Vibr. 1995;185(3):531-43.
- [84] Gry L. Dynamic modelling of railway track based on wave propagation. J Sound Vibr. 1996;195(3):477-505.
- [85] Han X, Liu GR, Xi ZC, Lam KY. Transient waves in a functionally graded cylinder. Int J Solids Struct. 2001;38(17):3021-37.
- [86] Hayashi T, Kawashima K, Sun ZQ, Rose JL. Analysis of flexural mode focusing by a semianalytical finite element method. J Acoust Soc Am. 2003;113(3):1241-8.
- [87] Taweel H, Dong SB, Kazic M. Wave reflection from the free end of a cylinder with an arbitrary cross-section. Int J Solids Struct. 2000;37(12):1701-26.
- [88] Mazzotti M, Marzani A, Bartoli I. Dispersion analysis of leaky guided waves in fluid-loaded waveguides of generic shape. Ultrasonics. 2014;54(1):408-18.
- [89] Gravenkamp H, Birk C, Song CM. Numerical modeling of elastic waveguides coupled to infinite fluid media using exact boundary conditions. Comput Struct. 2014;141:36-45.
- [90] Hayashi T, Inoue D. Calculation of leaky Lamb waves with a semi-analytical finite element method. Ultrasonics. 2014;54(6):1460-9.
- [91] Hladky-Hennion AC, Langlet P, Bossut R, De Billy M. Finite element modelling of radiating waves in immersed wedges. J Sound Vibr. 1998;212(2):265-74.
- [92] Guddati MN, Lim KW, Zahid MA. Perfectly matched discrete layers for unbounded domain modeling. In: Magoulès F, editor. Computational methods for acoustics problems. UK: Saxe-Coburg Publications; 2008. p. 69-98.
- [93] Guddati MN, Lim KW. Continued fraction absorbing boundary conditions for convex polygonal domains. Int J Numer Methods Eng. 2006;66(6):949-77.
- [94] Chew WC, Weedon WH. A 3d perfectly matched medium from modified maxwells equations with stretched coordinates. Microw Opt Technol Lett. 1994;7(13):599-604.
- [95] Guddati MN, Druskin V, Vaziri Astaneh A. Exponential convergence through linear finite element discretization of stratified subdomains. J Comput Phys. 2016;322:429–47.

- [96] Vaziri Astaneh A, Guddati MN. Efficient computation of dispersion curves for multilayered waveguides and half-spaces. Comput Meth Appl Mech Eng. 2016;300:27-46.
- [97] Vaziri Astaneh A, Guddati MN. WaveDisp software: http://waveDisp.com.
- [98] Vidal P, Polit O. A sine finite element using a zig-zag function for the analysis of laminated composite beams. Compos Pt B-Eng. 2011;42(6):1671-82.
- [99] Khandelwal RP, Chakrabarti A, Bhargava P. An efficient FE model and Least Square Error method for accurate calculation of transverse shear stresses in composites and sandwich laminates. Compos Pt B-Eng. 2012;43(4):1695-704.
- [100] Ferreira AJM, Araujo AL, Neves AMA, Rodrigues JD, Carrera E, Cinefra M, et al. A finite element model using a unified formulation for the analysis of viscoelastic sandwich laminates. Compos Pt B-Eng. 2013;45(1):1258-64.
- [101] Kargarnovin MH, Ahmadian MT, Jafari-Talookolaei RA, Abedi M. Semi-analytical solution for the free vibration analysis of generally laminated composite Timoshenko beams with single delamination. Compos Pt B-Eng. 2013;45(1):587-600.
- [102] Funari MF, Greco F, Lonetti P. A moving interface finite element formulation for layered structures. Compos Pt B-Eng. 2016;96:325-37.
- [103] Sause MGR, Hamstad MA, Horn S. Finite element modeling of lamb wave propagation in anisotropic hybrid materials. Compos Pt B-Eng. 2013;53:249-57.
- [104] Kumar SK, Cinefra M, Carrera E, Ganguli R, Harursampath D. Finite element analysis of free vibration of the delaminated composite plate with variable kinematic multilayered plate elements. Compos Pt B-Eng. 2014;66:453-65.
- [105] Mantari JL, Canales FG. Finite element formulation of laminated beams with capability to model the thickness expansion. Compos Pt B-Eng. 2016;101:107-15.
- [106] Vaziriastaneh A. On the forward and inverse computational wave propagation problems, PhD Thesis: North Carolina State University, Raleigh, USA; 2016.
- [107] Renno JM, Mace BR. On the forced response of waveguides using the wave and finite element method. J Sound Vibr. 2010;329(26):5474-88.
- [108] Chronopoulos D, Ichchou M, Troclet B, Bareille O. Computing the broadband vibroacoustic response of arbitrarily thick layered panels by a wave finite element approach. Appl Acoust. 2014;77:89-98.
- [109] Renno JM, Mace BR. Calculating the forced response of cylinders and cylindrical shells using the wave and finite element method. J Sound Vibr. 2014;333(21):5340-55.
- [110] Chronopoulos D. Wave steering effects in anisotropic composite structures: Direct calculation of the energy skew angle through a finite element scheme. Ultrasonics. 2017;73:43-8.
- [111] Savadatti S, Guddati MN. A finite element alternative to infinite elements. Comput Meth Appl Mech Eng. 2010;199(33-36):2204-23.
- [112] Mozhaev VG, Weihnacht M. Subsonic leaky Rayleigh waves at liquid-solid interfaces. Ultrasonics. 2002;40(1-8):927-33.
- [113] Yu L, Tian Z. Case study of guided wave propagation in a one-side water-immersed steel plate. Case Stud Nondestruct Test Eval. 2015;3:1-8.
- [114] Padilla F, de Billy M, Quentin G. Theoretical and experimental studies of surface waves on solid-fluid interfaces when the value of the fluid sound velocity is located between the shear and the longitudinal ones in the solid. J Acoust Soc Am. 1999;106(2):666-73.
- [115] Lee YC, Kuo SH. Leaky Lamb wave of a piezoelectric plate subjected to conductive fluid loading: Theoretical analysis and numerical calculation. J Appl Phys. 2006;100(7).
- [116] Vogt T, Lowe M, Cawley P. The scattering of guided waves in partly embedded cylindrical structures. J Acoust Soc Am. 2003;113(3):1258-72.
- [117] Caviglia G, Morro A. Inhomogeneous waves in solids and fluids. Farrer Road, Singapore: World scientific Co. Pte. Ltd.; 1992.
- [118] Agha YO, Zolla F, Nicolet A, Guenneau S. On the use of PML for the computation of leaky modes An application to microstructured optical fibres. Compel-Int J Comp Math Electr. 2008;27(1):95-109.
- [119] Vinh PC. Scholte-wave velocity formulae. Wave Motion. 2013;50(2):180-90.

- [120] Van de Rostyne K, Glorieux C, Gao WM, Lauriks W, Thoen J. Experimental investigation of leaky Lamb modes by an optically induced grating. IEEE Trans Ultrason Ferroelectr Freq Control. 2002;49(9):1245-53.
- [121] Teixeira FL, Chew WC. Perfectly matched layer in cylindrical coordinates. In: Proceedings of AP-S Int Symp. Canada, Conference, Conference 1997. p. 1908-11.
- [122] Gunawan A, Hirose S. Boundary element analysis of guided waves in a bar with an arbitrary cross-section. Eng Anal Bound Elem. 2005;29(10):913-24.
- [123] Chung CH, Lee YC. Fabrication of poly (vinylidene fluoride-trifluoroethylene) ultrasound focusing transducers and measurements of elastic constants of thin plates. NDT E Int. 2010;43(2):96-105.
- [124] Lin CI, Lu Y, He CF, Song GR, Lee YC. Measurement of circumferential Lamb waves using a line-focus poly(vinylidene fluoride) transducer and cross correlation waveform analysis. J Acoust Soc Am. 2015;138(5):2738-43.
- [125] Mazzotti M, Bartoli I, Marzani A. Ultrasonic leaky guided waves in fluid-coupled generic waveguides: hybrid finite-boundary element dispersion analysis and experimental validation. J Appl Phys. 2014;115(14):1-10.

Appendix A: Semi-discretization of 1D Waveguides in Cartesian coordinates

Expanding the governing equation in (1) by using (2) gives,

$$-\partial (\mathbf{D}_{zz}\partial \mathbf{u}/\partial z)/\partial z - \partial (\mathbf{D}_{zv}\partial \mathbf{u}/\partial y)/\partial z - \partial (\mathbf{D}_{zv}^{T}\partial \mathbf{u}/\partial z)/\partial y - \partial (\mathbf{D}_{w}\partial \mathbf{u}/\partial y)/\partial y - \rho_{S}\omega^{2}\mathbf{I}_{2\times2}\mathbf{u} = \mathbf{0}, \quad (A1)$$

where $\mathbf{D}_{pq} = (\mathbf{L}_p^S)^T \mathbf{D}_{3\times 3} \mathbf{L}_q^S$ for $p,q \in \{z,y\}$ and \mathbf{L}^S matrices are defined in (2). We use Fourier transform in the z direction and discretize the solid and fluid domains along the y direction, i.e. $\mathbf{u}(z,y,\omega) = \mathbf{N}_S(y) \bar{\mathbf{u}}(k_z,\omega) e^{ik_z z}$ and $p(z,y,\omega) = \mathbf{N}_F(y) \bar{p}(k_z,\omega) e^{ik_z z}$ where k_z is the wavenumber in the z direction. Shape function matrix is defined as the Kronecker product $\mathbf{N}_S = \bar{\mathbf{N}}_S \otimes \mathbf{I}_{2\times 2}$ where $\bar{\mathbf{N}}_S = [N_S^1,...,N_S^{m_S}]$ is the shape function vector for a 1D m_S -noded element in the solid domain $(y_1 \le y \le y_2)$ and $\mathbf{N}_F = [N_F^1,...,N_F^{m_F}]$ is the shape function vector for a 1D m_F -noded element in the fluid region $(y_2 \le y)$. The resulting quadratic eigenvalue problem can be written as,

$$\begin{bmatrix} k_z^2 \tilde{\mathbf{K}}^{S2} + i k_z \tilde{\mathbf{K}}^{S1} + \tilde{\mathbf{K}}^{S0} - \omega^2 \tilde{\mathbf{M}}^S & -\mathbf{C}_{SF} \\ -\omega^2 \mathbf{C}_{SF}^T & k_z^2 \mathbf{K}^{F2} + \mathbf{K}^{F0} - \omega^2 \mathbf{M}^F \end{bmatrix} \begin{bmatrix} \tilde{\mathbf{\phi}}_S \\ \mathbf{\phi}_F \end{bmatrix} = \begin{bmatrix} \mathbf{0} \\ \mathbf{0} \end{bmatrix}, \tag{A2}$$

where $\tilde{\mathbf{K}}^{S2} = \mathbf{K}_{zz}^S$, $\tilde{\mathbf{K}}^{S1} = (\mathbf{K}_{zy}^S)^T - \mathbf{K}_{zy}^S$, $\tilde{\mathbf{K}}^{S0} = \mathbf{K}_{yy}^S$, $\mathbf{K}^{F2} = \mathbf{K}_{zz}^F$ and $\mathbf{K}^{F0} = \mathbf{K}_{yy}^F$ with,

$$\mathbf{K}_{zz}^{S} = \int_{y_{1}}^{y_{2}} \mathbf{N}_{S}^{T} \mathbf{D}_{zz} \mathbf{N}_{S} \, dy, \qquad \mathbf{K}_{zy}^{S} = \int_{y_{1}}^{y_{2}} \mathbf{N}_{S}^{T} \mathbf{D}_{zy} \mathbf{B}_{S} dy, \qquad \mathbf{K}_{yy}^{S} = \int_{y_{1}}^{y_{2}} \mathbf{B}_{S}^{T} \mathbf{D}_{yy} \mathbf{B}_{S} dy,$$

$$\mathbf{M}^{S} = \int_{y_{1}}^{y_{2}} \mathbf{N}_{S}^{T} \rho_{S} \mathbf{N}_{S} \, dy, \qquad \mathbf{K}_{yy}^{F} = \int_{y_{2}}^{y_{3}} \mathbf{B}_{F}^{T} \rho_{F}^{-1} \mathbf{B}_{F} dy, \qquad \mathbf{K}_{zz}^{F} = \int_{y_{2}}^{y_{3}} \mathbf{N}_{F}^{T} \rho_{F}^{-1} \mathbf{N}_{F} dy,$$

$$\mathbf{M}^{F} = \int_{y_{2}}^{y_{3}} \mathbf{N}_{F}^{T} \rho_{F}^{-1} c_{F}^{-2} \mathbf{N}_{F} dy, \qquad \mathbf{C}_{SF} = \int_{y_{2}}^{y_{2}} \mathbf{N}_{S}^{T} \mathbf{n}_{f} \mathbf{N}_{F} dy,$$

$$(A3)$$

in which the shape function derivative matrix is defined as $\mathbf{B}_S = \overline{\mathbf{B}}_S \otimes \mathbf{I}_{2\times 2}$ where $\overline{\mathbf{B}}_S = [dN_S^1/dy,...,dN_S^{m_S}/dy]$ and $\mathbf{B}_F = [dN_F^1/dy,...,dN_F^{m_F}/dy]$ are the shape function derivative vectors

for the solid domain and fluid region, respectively. Also $\mathbf{n}_f = \{0 \pm 1\}^T$ is the unit normal for the solid-fluid interface using the appropriate sign at each interface. By rearranging the degrees of freedom (z then y), the quadratic eigenvalue problem in (A2) can be converted to a generalized eigenvalue problem in (4) with,

$$\mathbf{K}_{2}^{S} = \begin{bmatrix} \tilde{\mathbf{K}}_{zz}^{S2} \\ -\tilde{\mathbf{K}}_{yz}^{S1} & \tilde{\mathbf{K}}_{yy}^{S2} \end{bmatrix}, \quad \mathbf{K}_{0}^{S} = \begin{bmatrix} \tilde{\mathbf{K}}_{zz}^{S0} & \tilde{\mathbf{K}}_{zy}^{S1} \\ & \tilde{\mathbf{K}}_{yy}^{S0} \end{bmatrix}, \quad \mathbf{M}^{S} = \begin{bmatrix} \tilde{\mathbf{M}}_{zz}^{S} \\ & \tilde{\mathbf{M}}_{yy}^{S} \end{bmatrix},$$
(A4)

and $\phi_S = \{\tilde{\phi}_{S_2}^T \ ik_z \tilde{\phi}_{S_2}^T\}^T$. Note that the fluid contribution matrices in (A3) are only written for the top fluid half space $(y_2 \le y)$. The associated matrices and interaction terms have to be considered for the bottom fluid half space $(y \le y_1)$, if exists. Also note that the size of the generalized eigenvalue problem in (4) is the same as the quadratic eigenvalue problem in (A2).

Appendix B: Semi-discretization of 1D Waveguides in cylindrical coordinates

Expanding the governing equation in (1) by using (12) gives,

$$-r^{-1}\partial(\mathbf{D}_{rr}r\partial\mathbf{u}/\partial r)/\partial r - r^{-1}\partial(\mathbf{D}_{r\theta}\partial\mathbf{u}/\partial \theta)/\partial r - r^{-1}\partial(\mathbf{D}_{rz}r\partial\mathbf{u}/\partial z)/\partial r - r^{-1}\partial(\mathbf{D}_{ro}\mathbf{u})/\partial r$$

$$-r^{-1}\partial(\mathbf{D}_{r\theta}^{T}\partial\mathbf{u}/\partial r)/\partial \theta - r^{-1}\partial(\mathbf{D}_{\theta\theta}r^{-1}\partial\mathbf{u}/\partial \theta)/\partial \theta - r^{-1}\partial(\mathbf{D}_{\theta z}\partial\mathbf{u}/\partial z)/\partial \theta - r^{-1}\partial(\mathbf{D}_{\theta o}r^{-1}\mathbf{u})/\partial \theta$$

$$-\partial(\mathbf{D}_{rz}^{T}\partial\mathbf{u}/\partial r)/\partial z - \partial(\mathbf{D}_{\theta z}^{T}r^{-1}\partial\mathbf{u}/\partial \theta)/\partial z - \partial(\mathbf{D}_{zz}\partial\mathbf{u}/\partial z)/\partial z - \partial(\mathbf{D}_{zo}r^{-1}\mathbf{u})/\partial z$$

$$+r^{-1}(\mathbf{D}_{ro}^{T})\partial\mathbf{u}/\partial r + r^{-1}(\mathbf{D}_{\theta o}^{T}r^{-1})\partial\mathbf{u}/\partial \theta + r^{-1}(\mathbf{D}_{zo}^{T})\partial\mathbf{u}/\partial z + r^{-1}(\mathbf{D}_{oo}r^{-1})\mathbf{u} - \rho_{S}\omega^{2}\mathbf{I}_{3\times3}\mathbf{u} = \mathbf{0}$$
(B1)

where $\mathbf{D}_{pq} = (\mathbf{L}_p^S)^T \mathbf{D}_{6\times 6} \mathbf{L}_q^S$ for $p,q \in \{r,\theta,z,o\}$ and \mathbf{L}^S matrices are defined in (12). We use Fourier series in θ , Fourier transform in the z direction, and discretize the solid and fluid domains along the r direction, i.e. $\mathbf{u}(r,\theta,z,\omega) = \mathbf{N}_S(r) \overline{\mathbf{u}}(n,k_z,\omega) e^{in\theta+ik_z z}$ and $p(r,\theta,z,\omega) = \mathbf{N}_F(r) \overline{p}(n,k_z,\omega) e^{in\theta+ik_z z}$ where k_z is the axial wavenumber and n is the circumferential Fourier number. The shape function matrix is defined as the Kronecker product $\mathbf{N}_S = \overline{\mathbf{N}}_S \otimes \mathbf{I}_{3\times 3}$ where $\overline{\mathbf{N}}_S = [N_S^1, ..., N_S^{m_S}]$ is the shape function vector for a 1D m_S -noded element in the solid domain $(r_1 \le r \le r_2)$ and $\mathbf{N}_F = [N_F^1, ..., N_F^{m_F}]$ is the shape function vector for a 1D m_F -noded element in the fluid region $(r_2 \le r)$. Resulting quadratic eigenvalue problem is similar to (A2) where $\widetilde{\mathbf{K}}^{S2} = \mathbf{K}_{zz}^S$, $\widetilde{\mathbf{K}}^{S0} = \mathbf{K}_{rr}^S + \mathbf{K}_{ro}^S + (\mathbf{K}_{ro}^S)^T + \mathbf{K}_{oo}^S + in(\mathbf{K}_{r\theta}^S - (\mathbf{K}_{r\theta}^S)^T + (\mathbf{K}_{\theta o}^S)^T - \mathbf{K}_{\theta o}^S) + n^2 \mathbf{K}_{\theta o}^S$, $\mathbf{K}^{F2} = \mathbf{K}_{rr}^F + n^2 \mathbf{K}_{\theta \theta}^F$ and $\widetilde{\mathbf{K}}^{S1} = \mathbf{K}_{rr}^S - (\mathbf{K}_{ro}^S)^T - \mathbf{K}_{zo}^S + (\mathbf{K}_{zo}^S)^T - in(\mathbf{K}_{\theta z}^S + (\mathbf{K}_{\theta z}^S)^T)$ with,

$$\mathbf{K}_{rr}^{S} = \int_{r_{1}}^{r_{2}} \mathbf{B}_{S}^{T} \mathbf{D}_{rr} \mathbf{B}_{S} r dr, \qquad \mathbf{K}_{r\theta}^{S} = \int_{r_{1}}^{r_{2}} \mathbf{B}_{S}^{T} r^{-1} \mathbf{D}_{r\theta} \mathbf{N}_{S} r dr, \qquad \mathbf{K}_{rz}^{S} = \int_{r_{1}}^{r_{2}} \mathbf{B}_{S}^{T} \mathbf{D}_{rz} \mathbf{N}_{S} r dr,$$

$$\mathbf{K}_{ro}^{S} = \int_{r_{1}}^{r_{2}} \mathbf{B}_{S}^{T} r^{-1} \mathbf{D}_{ro} \mathbf{N}_{S} r dr, \qquad \mathbf{K}_{\theta\theta}^{S} = \int_{r_{1}}^{r_{2}} \mathbf{N}_{S}^{T} r^{-2} \mathbf{D}_{\theta\theta} \mathbf{N}_{S} r dr, \qquad \mathbf{K}_{\theta z}^{S} = \int_{r_{1}}^{r_{2}} \mathbf{N}_{S}^{T} r^{-1} \mathbf{D}_{\theta z} \mathbf{N}_{S} r dr,$$

$$\mathbf{K}_{\theta o}^{S} = \int_{r_{1}}^{r_{2}} \mathbf{N}_{S}^{T} r^{-2} \mathbf{D}_{\theta o} \mathbf{N}_{S} r dr, \qquad \mathbf{K}_{zz}^{S} = \int_{r_{1}}^{r_{2}} \mathbf{N}_{S}^{T} \mathbf{D}_{zz} \mathbf{N}_{S} r dr, \qquad \mathbf{K}_{zo}^{S} = \int_{r_{1}}^{r_{2}} \mathbf{N}_{S}^{T} r^{-1} \mathbf{D}_{zo} \mathbf{N}_{S} r dr,$$

$$\mathbf{K}_{oo}^{S} = \int_{r_{1}}^{r_{2}} \mathbf{N}_{S}^{T} r^{-2} \mathbf{D}_{oo} \mathbf{N}_{S} r dr, \qquad \mathbf{K}_{zz}^{F} = \int_{r_{2}}^{r_{3}} \mathbf{N}_{S}^{T} \rho_{S} \mathbf{N}_{S} r dr, \qquad \mathbf{K}_{rr}^{F} = \int_{r_{2}}^{r_{3}} \mathbf{B}_{F}^{T} \rho_{F}^{-1} \mathbf{B}_{F} r dr,$$

$$\mathbf{K}_{\theta\theta}^{F} = \int_{r_{2}}^{r_{3}} \mathbf{N}_{F}^{T} \rho_{F}^{-1} r^{-2} \mathbf{N}_{F} r dr, \qquad \mathbf{K}_{zz}^{F} = \int_{r_{2}}^{r_{3}} \mathbf{N}_{F}^{T} \rho_{F}^{-1} \mathbf{N}_{F} r dr, \qquad \mathbf{M}^{F} = \int_{r_{2}}^{r_{3}} \mathbf{N}_{F}^{T} \rho_{F}^{-1} c_{F}^{-2} \mathbf{N}_{F} r dr,$$

$$\mathbf{C}_{SF} = \int_{r_{2}}^{r_{2}} \mathbf{N}_{S}^{T} \mathbf{n}_{f} \mathbf{N}_{F} r dr,$$

in which the shape function derivative matrix is defined as $\mathbf{B}_S = \overline{\mathbf{B}}_S \otimes \mathbf{I}_{3\times 3}$ where $\overline{\mathbf{B}}_S = [dN_S^1 / dr, ..., dN_S^{m_S} / dr]$ and $\mathbf{B}_F = [dN_F^1 / dr, ..., dN_F^{m_F} / dr]$ are the shape function derivative vectors for the solid domain and fluid region, respectively. Also $\mathbf{n}_f = \{\pm 1 \ 0 \ 0\}^T$ is the unit normal for the solid-fluid interface using the appropriate sign at each interface. By rearranging the degrees of freedom (r then θ and z), the quadratic eigenvalue problem in (A2) can be converted to the generalized eigenvalue problem in (4) with,

$$\mathbf{K}_{2}^{S} = \begin{bmatrix} \tilde{\mathbf{K}}_{rr}^{S2} & \mathbf{0} & -\tilde{\mathbf{K}}_{rz}^{S1} \\ \mathbf{0} & \tilde{\mathbf{K}}_{\theta\theta}^{S2} & -\tilde{\mathbf{K}}_{\thetaz}^{S1} \\ \mathbf{0} & \mathbf{0} & \tilde{\mathbf{K}}_{zz}^{S2} \end{bmatrix}, \quad \mathbf{K}_{0}^{S} = \begin{bmatrix} \tilde{\mathbf{K}}_{rr}^{S0} & \tilde{\mathbf{K}}_{r\theta}^{S0} & \mathbf{0} \\ \tilde{\mathbf{K}}_{\theta r}^{S0} & \tilde{\mathbf{K}}_{\theta\theta}^{S0} & \mathbf{0} \\ \tilde{\mathbf{K}}_{zr}^{S1} & \tilde{\mathbf{K}}_{z\theta}^{S1} & \tilde{\mathbf{K}}_{zz}^{S0} \end{bmatrix},$$
(B3)

and $\phi_S = \{ik_z\tilde{\phi}_{Sr}^T \quad ik_z\tilde{\phi}_{S\theta}^T \quad \tilde{\phi}_{Sz}^T \}^T$. Again, the size of the generalized eigenvalue problem is the same as the original quadratic eigenvalue problem. Note that the fluid contribution matrices in (B2) are only defined for the exterior fluid half-space $(r_2 \le r)$. The associated matrices and interaction terms have to be considered for the fluid inside the pipe $(r \le r_1)$, if exists.

Appendix C: Semi-discretization of 2D Waveguides in Cartesian coordinates

Expanding the governing equation in (1) by using (15) gives,

$$-\partial (\mathbf{D}_{xx}\partial \mathbf{u} / \partial x) / \partial x - \partial (\mathbf{D}_{xy}\partial \mathbf{u} / \partial y) / \partial x - \partial (\mathbf{D}_{xz}\partial \mathbf{u} / \partial z) / \partial x$$

$$-\partial (\mathbf{D}_{xy}^T \partial \mathbf{u} / \partial x) / \partial y - \partial (\mathbf{D}_{yy}\partial \mathbf{u} / \partial y) / \partial y - \partial (\mathbf{D}_{yz}\partial \mathbf{u} / \partial z) / \partial y$$

$$-\partial (\mathbf{D}_{xz}^T \partial \mathbf{u} / \partial x) / \partial z - \partial (\mathbf{D}_{yz}^T \partial \mathbf{u} / \partial y) / \partial z - \partial (\mathbf{D}_{zz}\partial \mathbf{u} / \partial z) / \partial z - \rho_S \omega^2 \mathbf{I}_{3\times 3} \mathbf{u} = \mathbf{0}$$
(C1)

where $\mathbf{D}_{pq} = (\mathbf{L}_p^S)^T \mathbf{D}_{6\times 6} \mathbf{L}_q^S$ for $p,q \in \{x,y,z\}$ and \mathbf{L}^S matrices are defined in (15). We use Fourier transform in the z direction and discretize the solid and fluid domains in the x-y plane, i.e. $\mathbf{u}(x,y,z,\omega) = \mathbf{N}_S(x,y) \overline{\mathbf{u}}(k_z,\omega) e^{ik_z z}$ and $p(x,y,z,\omega) = \mathbf{N}_F(x,y) \overline{p}(k_z,\omega) e^{ik_z z}$ where k_z is the axial wavenumber. Shape function matrix is defined as the Kronecker product $\mathbf{N}_S = \overline{\mathbf{N}}_S \otimes \mathbf{I}_{3\times 3}$ where $\overline{\mathbf{N}}_S = [N_S^1,...,N_S^{m_S}]$ is the shape function vector for a 2D m_S -noded element in the solid domain and

 $\begin{aligned} \mathbf{N}_F = & [N_F^1, ..., N_F^{m_F}] \text{ is the shape function vector for a 2D } m_F \text{-noded element in the fluid region. The} \\ & \text{resulting quadratic eigenvalue problem is similar to (A2) where } \tilde{\mathbf{K}}^{S2} = & \mathbf{K}_{zz}^S \\ & \tilde{\mathbf{K}}^{S1} = & \mathbf{K}_{xz}^S - (\mathbf{K}_{xz}^S)^T + \mathbf{K}_{yz}^S - (\mathbf{K}_{yz}^S)^T \\ & \tilde{\mathbf{K}}^{S0} = & \mathbf{K}_{xx}^S + \mathbf{K}_{yy}^S + \mathbf{K}_{xy}^S + (\mathbf{K}_{xy}^S)^T \\ & \mathbf{K}^{F2} = & \mathbf{K}_{zz}^F \\ & \text{and } \mathbf{K}^{F0} = & \mathbf{K}_{xy}^F \end{aligned}$

$$\mathbf{K}_{xx}^{S} = \int_{\Omega} \mathbf{B}_{Sx}^{T} \mathbf{D}_{xx} \mathbf{B}_{Sx} d\Omega, \qquad \mathbf{K}_{xy}^{S} = \int_{\Omega} \mathbf{B}_{Sx}^{T} \mathbf{D}_{xy} \mathbf{B}_{Sy} d\Omega, \qquad \mathbf{K}_{xz}^{S} = \int_{\Omega} \mathbf{B}_{Sx}^{T} \mathbf{D}_{xz} \mathbf{N}_{S} d\Omega,$$

$$\mathbf{K}_{yy}^{S} = \int_{\Omega} \mathbf{B}_{Sy}^{T} \mathbf{D}_{yy} \mathbf{B}_{Sy}^{T} d\Omega, \qquad \mathbf{K}_{yz}^{S} = \int_{\Omega} \mathbf{B}_{Sy}^{T} \mathbf{D}_{yz} \mathbf{N}_{S} d\Omega, \qquad \mathbf{K}_{zz}^{S} = \int_{\Omega} \mathbf{N}_{S}^{T} \mathbf{D}_{zz} \mathbf{N}_{S} d\Omega,$$

$$\mathbf{M}^{S} = \int_{\Omega} \mathbf{N}_{S}^{T} \rho_{S} \mathbf{N}_{S} d\Omega, \qquad \mathbf{K}_{xy}^{F} = \int_{\Omega} \mathbf{B}_{F}^{T} \rho_{F}^{-1} \mathbf{B}_{F} d\Omega, \qquad \mathbf{K}_{zz}^{F} = \int_{\Omega} \mathbf{N}_{F}^{T} \rho_{F}^{-1} \mathbf{N}_{F} d\Omega,$$

$$\mathbf{M}^{F} = \int_{\Omega} \mathbf{N}_{F}^{T} \rho_{F}^{-1} c_{F}^{-2} \mathbf{N}_{F} d\Omega, \qquad \mathbf{C}_{SF} = \int_{\Gamma} \mathbf{N}_{S}^{T} \mathbf{n}_{f} \mathbf{N}_{F} d\Gamma,$$

$$(C2)$$

in which the shape-function-derivative matrix is defined as $\mathbf{B}_{Sx} = \overline{\mathbf{B}}_{Sx} \otimes \mathbf{I}_{3\times3}$, $\mathbf{B}_{Sy} = \overline{\mathbf{B}}_{Sy} \otimes \mathbf{I}_{3\times3}$ where $\overline{\mathbf{B}}_{Sx} = [dN_S^1 / dx, ..., dN_S^{m_S} / dx]$, $\overline{\mathbf{B}}_{Sy} = [dN_S^1 / dy, ..., dN_S^{m_S} / dy]$ and $\mathbf{B}_F = [dN_F^1 / dx, ..., dN_F^{m_F} / dx;$ $dN_F^1 / dy, ..., dN_F^{m_F} / dy]$ are the shape-function-derivative vectors for the solid and fluid domains, respectively. Also $\mathbf{n}_f = \{n_1 \ n_2 \ 0\}^T$ is the unit normal for the fluid at each interface. By rearranging the degrees of freedom (x then y and z), the quadratic eigenvalue problem in (A2) can be converted to the generalized eigenvalue problem in (4) with,

$$\mathbf{K}_{2}^{S} = \begin{bmatrix} \tilde{\mathbf{K}}_{xx}^{S2} & \mathbf{0} & -\tilde{\mathbf{K}}_{xz}^{S1} \\ \mathbf{0} & \tilde{\mathbf{K}}_{yy}^{S2} & -\tilde{\mathbf{K}}_{yz}^{S1} \\ \mathbf{0} & \mathbf{0} & \tilde{\mathbf{K}}_{zz}^{S2} \end{bmatrix}, \quad \mathbf{K}_{0}^{S} = \begin{bmatrix} \tilde{\mathbf{K}}_{xx}^{S0} & \tilde{\mathbf{K}}_{xy}^{S0} & \mathbf{0} \\ \tilde{\mathbf{K}}_{yx}^{S0} & \tilde{\mathbf{K}}_{yy}^{S0} & \mathbf{0} \\ \tilde{\mathbf{K}}_{zx}^{S1} & \tilde{\mathbf{K}}_{zy}^{S1} & \tilde{\mathbf{K}}_{zz}^{S0} \end{bmatrix},$$
(C3)

and $\phi_S = \{ik_z \tilde{\phi}_{Sx}^T \quad ik_z \tilde{\phi}_{Sy}^T \quad \tilde{\phi}_{Sz}^T \}^T$.